Article

Cell Metabolism

Hepatocyte TAZ/WWTR1 Promotes Inflammation and Fibrosis in Nonalcoholic Steatohepatitis

Graphical Abstract

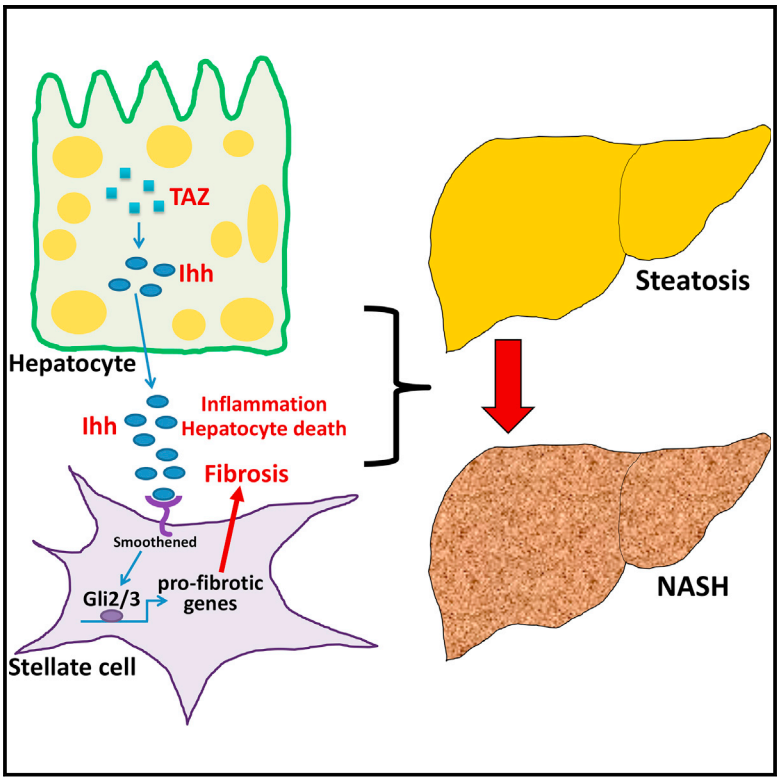

Authors

Xiaobo Wang, Ze Zheng, Jorge Matias Caviglia, ..., Jay H. Lefkowitch, Robert F. Schwabe, Ira Tabas

Correspondence

xw2279@columbia.edu (X.W.), iat1@columbia.edu (I.T.)

In Brief

Hepatic fibrosis is a key feature of nonalcoholic steatohepatitis (NASH) affecting morbidity. Wang et al. investigate the underlying mechanisms for progression from benign steatosis to NASH and show that the transcription factor TAZ/WWTR1 is increased in mouse and human NASH. Silencing TAZ can prevent or reverse NASH features, notably fibrosis.

Highlights

- TAZ/WWTR1 is increased in hepatocytes in human and mouse NASH liver
- Hepatocyte TAZ silencing in steatosis blocks inflammation, cell death, and fibrosis
- Hepatocyte TAZ silencing in NASH reverses inflammation, cell death, and fibrosis
- Hepatocyte TAZ promotes fibrosis by inducing Ihh, a hepatic stellate cell activator

Wang et al., 2016, Cell Metabolism *24*, 1–15
December 13, 2016
http://dx.doi.org/10.1016/j.cmet.2016.09.016

CellPress

Please cite this article in press as: Wang et al., Hepatocyte TAZ/WWTR1 Promotes Inflammation and Fibrosis in Nonalcoholic Steatohepatitis, Cell Metabolism (2016), http://dx.doi.org/10.1016/j.cmet.2016.09.016

Cell Metabolism
Article

Hepatocyte TAZ/WWTR1 Promotes Inflammation and Fibrosis in Nonalcoholic Steatohepatitis

Xiaobo Wang,[1,*] Ze Zheng,[1] Jorge Matias Caviglia,[1,2] Kathleen E. Corey,[3,4] Tina M. Herfel,[5] Bishuang Cai,[1] Ricard Masia,[4,6] Raymond Chung,[3,4] Jay H. Lefkowitch,[7] Robert F. Schwabe,[1,2] and Ira Tabas[1,7,8,9,*]
[1]Department of Medicine
[2]Institute of Human Nutrition
Columbia University, New York, NY 10032, USA
[3]Gastrointestinal Unit, Massachusetts General Hospital, Boston, MA, 02114, USA
[4]Harvard Medical School, Boston, MA 02115, USA
[5]Teklad Diets, Envigo, Madison, WI, 53713, USA
[6]Department of Pathology and Laboratory Medicine, Massachusetts General Hospital, Boston, MA, 02114, USA
[7]Department of Pathology and Cell Biology
[8]Department of Physiology and Cellular Biophysics
Columbia University, New York, NY 10032, USA
[9]Lead Contact
*Correspondence: xw2279@columbia.edu (X.W.), iat1@columbia.edu (I.T.)
http://dx.doi.org/10.1016/j.cmet.2016.09.016

SUMMARY

Nonalcoholic steatohepatitis (NASH) is a leading cause of liver disease worldwide. However, the molecular basis of how benign steatosis progresses to NASH is incompletely understood, which has limited the identification of therapeutic targets. Here we show that the transcription regulator TAZ (WWTR1) is markedly higher in hepatocytes in human and murine NASH liver than in normal or steatotic liver. Most importantly, silencing of hepatocyte TAZ in murine models of NASH prevented or reversed hepatic inflammation, hepatocyte death, and fibrosis, but not steatosis. Moreover, hepatocyte-targeted expression of TAZ in a model of steatosis promoted NASH features, including fibrosis. In vitro and in vivo mechanistic studies revealed that a key mechanism linking hepatocyte TAZ to NASH fibrosis is TAZ/TEA domain (TEAD)-mediated induction of Indian hedgehog (Ihh), a secretory factor that activates fibrogenic genes in hepatic stellate cells. In summary, TAZ represents a previously unrecognized factor that contributes to the critical process of steatosis-to-NASH progression.

INTRODUCTION

The epidemic of obesity has led to the occurrence of fatty liver, or steatosis, in hundreds of millions of people worldwide. While simple steatosis is a relatively benign condition, approximately 20%–30% of these subjects will develop liver inflammation, dysfunctional fibrosis, and hepatocyte death, a serious condition known as nonalcoholic steatohepatitis (NASH) (Rinella, 2015). NASH can progress to cirrhotic liver disease and hepatocellular carcinoma and has become the leading cause of liver failure (Corey and Kaplan, 2014; Rinella, 2015). Despite the high prevalence and clinical importance of NASH, many gaps remain in our understanding of its pathophysiology, leading to a lack of mechanism-based therapeutic targets and treatment options (White et al., 2012).

NASH most likely develops as a result of multiple hits (Day and James, 1998), including obesity/insulin resistance-mediated steatosis and other insults that promote inflammation, fibrosis, and hepatocyte death (Singh et al., 2015). However, the molecular mechanisms corresponding to these pathogenic processes and their integration are poorly understood. In particular, there is a great need to elucidate the mechanisms leading to hepatic fibrosis, which is the leading determinant of long-term mortality in patients with NASH (Angulo et al., 2015a, 2015b; Puche et al., 2013). Extensive data indicate that activation of hepatic stellate cells (HSCs) plays a key role in NASH fibrosis (Mederacke et al., 2013), and although a number of factors have been proposed to activate HSCs in NASH, the work in this area is far from complete and has not yet led to FDA-approved treatment strategies (Angulo et al., 2015b; Puche et al., 2013).

In this context, we became interested in the Hippo pathway transcriptional activator TAZ (also known as WWTR1), which has been shown to have a pathophysiologic role in fibrosis in the lung (Liu et al., 2015). TAZ and the related protein YAP are orthologs of *Drosophila Yorkie*, a regulator of gene transcription that promotes tumor development in flies (Zanconato et al., 2016; Zhao et al., 2010). Although the roles of TAZ/YAP in normal physiology in mammals appear modest, they have emerged as key factors in carcinogenesis, tumor progression, and metastasis. At a cell biological level, TAZ/YAP mediate cellular responses to both intracellular shape changes and changes in the extracellular matrix environment. In the basal state, TAZ/YAP are relatively inactive as nuclear transcriptional regulators, because kinases in the so-called Hippo pathway maintain

TAZ/YAP in their phosphorylated, cytoplasmic state. Through dephosphorylation and other processes, however, TAZ/YAP translocate to the nucleus and become active transcriptional regulators. In the nucleus, they interact with TEA domain (TEAD) proteins, leading to transcription of genes possessing consensus TEAD-binding *cis*-regulatory sequences in promoter and enhancer regions.

While there are some hints in the literature that TAZ or YAP may be involved in various liver processes, their possible role in fatty liver disease or NASH progression has not been reported. We now demonstrate that TAZ expression is elevated in the livers of humans with NASH-related fibrosis and in the livers of several murine NASH models. Silencing of hepatocyte Taz in NASH mice prevents and even reverses the development of liver inflammation and fibrosis without affecting steatosis, and forced expression of TAZ in hepatocytes can promote the progression of NASH from steatosis. In vitro, conditioned medium from Taz-silenced versus control hepatocytes decreases fibrotic responses in hepatic stellate cells (HSCs), which we link both in vitro and in vivo in murine NASH to decreased hepatocyte secretion of the TAZ/TEAD target Indian hedgehog (Ihh). Thus, TAZ promotes NASH progression, including fibrosis, and therefore emerges as a potential therapeutic target to prevent the progression of steatosis to NASH.

RESULTS

TAZ Levels Are Increased in the Livers of Humans and Mice with NASH

We conducted TAZ immunofluorescence microscopy on human liver samples from obese individuals with normal, steatotic, and NASH histology. While there was similar TAZ staining in normal and steatotic livers, we observed a significant increase in TAZ staining in the NASH samples (Figure 1A). The specificity of the anti-human TAZ antibody for immunofluorescence is demonstrated by a silencing RNA-targeting Taz (siTaz) experiment conducted with human HepG2 liver cells (Figure S1A). TAZ localization in NASH liver was not confined to any one zone (Figure S1B), and most of the TAZ-stained cells were hepatocytes, as identified by HNF4α staining (Figure S1C). We then analyzed TAZ protein by immunoblot in liver extracts from subjects with NASH versus early non-alcoholic fatty liver disease (NAFLD) and normal liver and found that TAZ was expressed at the highest level in NASH liver (Figure 1B).

In preparation for TAZ causation studies, we explored TAZ expression in various mouse models of NASH. We began with the widely used methionine/choline-deficient (MCD) diet model, which induces NASH-like liver pathology despite weight loss and insulin sensitivity (Hebbard and George, 2011), and found that TAZ expression was markedly higher in MCD liver compared with control liver (Figure 1C). We next sought to study TAZ in a NASH model that had weight gain and insulin resistance, as is the case with humans. For this purpose, we modified two previously described diet-induced weight-gain models (Charlton et al., 2011; Kohli et al., 2010) to achieve NASH features within an experimentally acceptable time frame. We devised a diet that was rich in fructose, palmitate, cholesterol (FPC), and trans-fat, with other features as detailed in Tables S1 and S2. Cholesterol (1.2% by food weight) was added to the diet in view of multiple links between liver cholesterol and NASH in humans (Ioannou, 2016). Note that a high dietary content of cholesterol is needed to achieve adequately increased cholesterol absorption in C57BL/6J mice, the strain used here (Jolley et al., 1999).

After 16 weeks, FPC-fed mice had higher body weight and liver:body weight ratio than chow-fed mice (Figures S2A and S2B). Additionally, FPC mice showed significant increases in fasting blood glucose, plasma insulin, and alanine aminotransferase (ALT) and aspartate aminotransferase (AST) levels (Figures S2C–S2E). Analyses of liver sections revealed that the following parameters were greater in the livers of FPC-fed mice versus chow-fed mice: lipid droplet area (H&E and Oil Red O [ORO]), inflammatory cells, fibrosis (aniline blue component of trichrome [Trichr] and Sirius red [Sir red]), and cell death (TUNEL) (Figures S2F–S2K). As further evidence of inflammation, FPC liver had elevated liver mRNA levels for *Tnfa*, *Mcp1*, and *F4/80* (*Adgre1*; macrophages) and a higher percentage of F4/80$^+$ cells (Figures S2L and S2M). With regard to fibrosis-associated parameters, hepatic*Tgfb1* and *Acta2* (α-smooth muscle actin, α-SMA) mRNAs were higher in FPC-fed mice compared with chow-fed mice (Figure S2N), and there was also an increase in α-SMA$^+$ cells (Figures S2O). Moreover, as designed, liver cholesterol was elevated in the livers of FPC mice (Figures S2P and S2Q). Additional features of the model in terms of blood parameters and liver assays are shown in Figure S3, and Table S3 shows hepatic fatty acid changes similar to those reported for human NASH liver (Yamada et al., 2015). Finally, Figures S4A–S4G show a direct comparison with one of the models from which it was derived, referred to as the "fast food" (FF) model (Charlton et al., 2011).

Most importantly, for the purpose of our study, the livers of FPC mice express high levels of TAZ protein and *Wwtr1* (Taz) mRNA (Figures 1D and 1E). By immunoblot analysis, TAZ was abundant in extracts of primary hepatocytes from FPC-fed mice, but it could not be detected in extracts of combined non-hepatocytes (Figure S4H). Moreover, in view of the fact that the transcriptionally active form of TAZ is non-phosphorylated and nuclear (Liu et al., 2011), we found that the livers of FPC-fed mice had a lower phospho-TAZ:total TAZ ratio and higher nuclear TAZ compared with the livers of chow-fed mice (Figures S4I and S4J). Collectively, these data show that hepatocyte TAZ is induced in the livers of humans and mice with NASH, which led us to explore the possibility that TAZ may be a contributor to the progression from benign steatosis to NASH.

TAZ Silencing in Hepatocytes Suppresses Liver Inflammation, Fibrosis, and Cell Death in Mouse Models of NASH

To study TAZ function in NASH development, we used an adeno-associated virus type 8 vector in which short hairpin RNA-targeting Taz (shTaz) was driven by the H1 promoter (AAV8-H1-shTaz), which was designed to silence genes in liver (Lisowski et al., 2014). (NB: to conform to the literature, we use the common name Taz, rather than *Wwtr1*, for sh terminology.) Compared with AAV8-H1 control vector, AAV8-H1-shTaz led to robust silencing of TAZ (Figure 2A) and a decrease in the known TAZ/TEAD transcriptional targets, *Birc5* and *Rhamm* (Figure S5A).

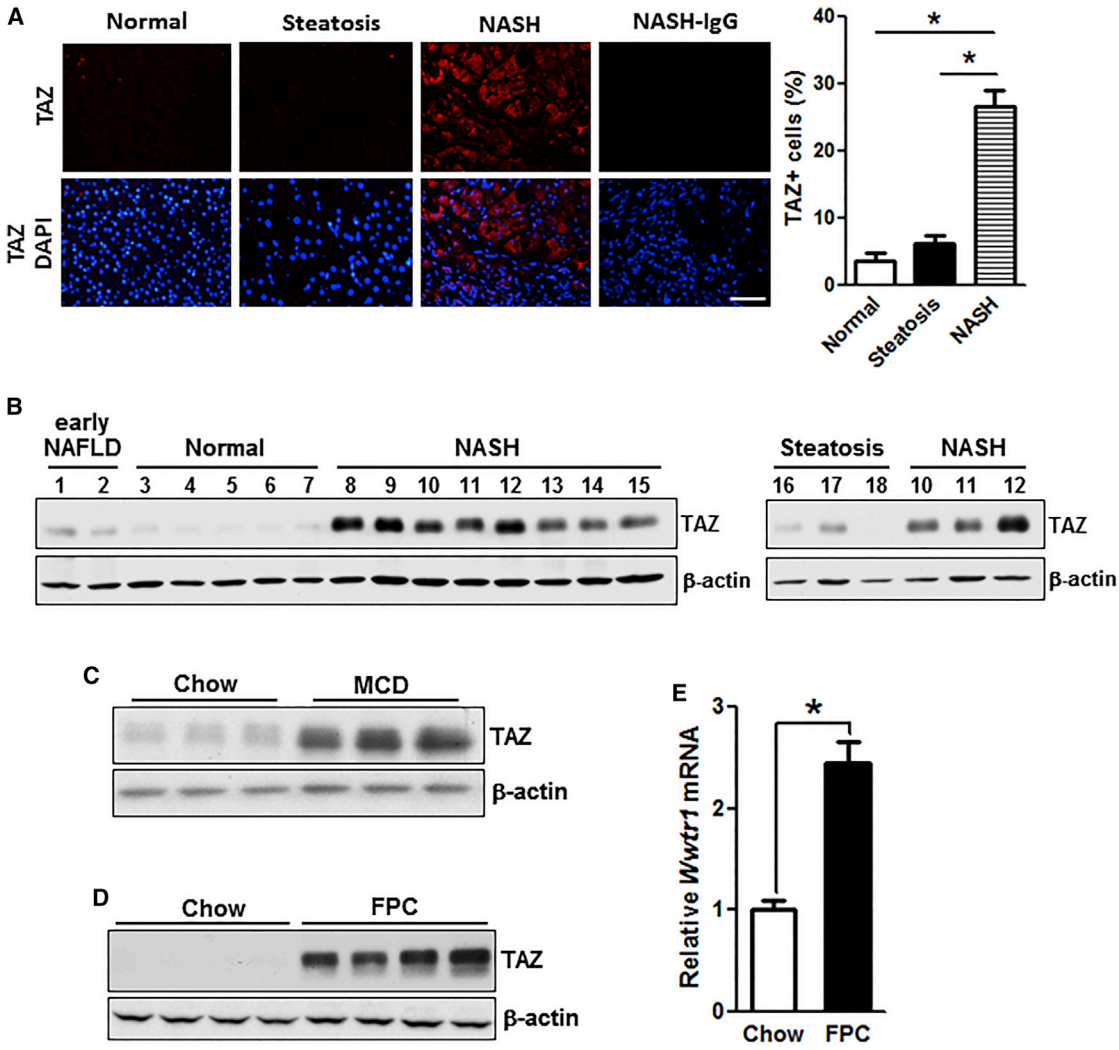

Figure 1. TAZ Levels Are Increased in the Livers of Humans and Mice with NASH

(A) TAZ immunofluorescence (red) in normal, steatotic, and NASH human liver sections; DAPI counterstain for nuclei is shown in bottom panels. NASH-IgG refers to control for primary antibody. Bar, 100 μm. The data were quantified as percent TAZ$^+$ cells relative to total liver cells (*$p < 0.0001$; mean ± SEM; n = 7 specimens/group).

(B) Immunoblots of TAZ in early NAFLD, normal, NASH, and steatotic human liver. For sake of comparison, samples 10–12 of NASH from the left blot were re-run with the steatosis samples in the right blot. β-actin was used as loading control.

(C) Immunoblot of liver TAZ in mice fed chow or MCD diet, with β-actin as loading control.

(D) Immunoblot of liver TAZ in mice fed chow or FPC diet, with β-actin as loading control.

(E) Quantification of *Wwtr1* (Taz) mRNA in livers from mice fed chow or FPC diet (*$p < 0.0001$; mean ± SEM; n = 6 mice/group)

In terms of specificity within the liver, note that TAZ expression in NASH liver was abundant in hepatocytes but not detected by immunoblot in combined non-hepatocytes (above). In extracts of adipose, heart, lung, and skeletal muscle, TAZ was not decreased in mice treated with AAV8-H1-shTaz; note that TAZ was not detected in kidney extract (Figure S5B).

Mouse body weight, liver:body weight ratio, fasting blood glucose, plasma insulin, and plasma cholesterol were similar in the shTaz and control groups (Figures S5C–S5G). Liver sections showed marked reductions in both inflammatory cell infiltration and fibrosis endpoints in the shTaz cohort (Figures 2B–2D), as reflected in fibrosis stage and NAFLD activity score (NAS) (Figures S5H and S5I), while steatosis was not affected (Figure S5J). Plasma ALT was decreased in shTaz-treated mice (Figure 2E), and this was associated with a decrease in TUNEL$^+$ and 4-HNE$^+$ liver cells (Figure 2F; Figure S5K), indicating that Taz silencing reduced both cell death and oxidative stress in liver cells. At the mRNA level, Taz silencing caused a robust reduction in the expression of mRNAs related to hepatic inflammation—*Tnfa*, *Mcp1*, and *F4/80* (*Adgre1*)—and fibrosis (Figures 2G and 2H), including the NASH-relevant genes *Acta2* (α-SMA), *Timp1*, *Des*, *Col1a1*, *Col1a2*, *Col3a1*, and *Vim* (Friedman, 2008; Younossi et al., 2011). These changes were accompanied by decreases in both F4/80$^+$ macrophages and α-SMA$^+$ cells (Figures 2I and 2J; Figure S5L). Note that silencing TAZ did not change filipin staining of liver, suggesting

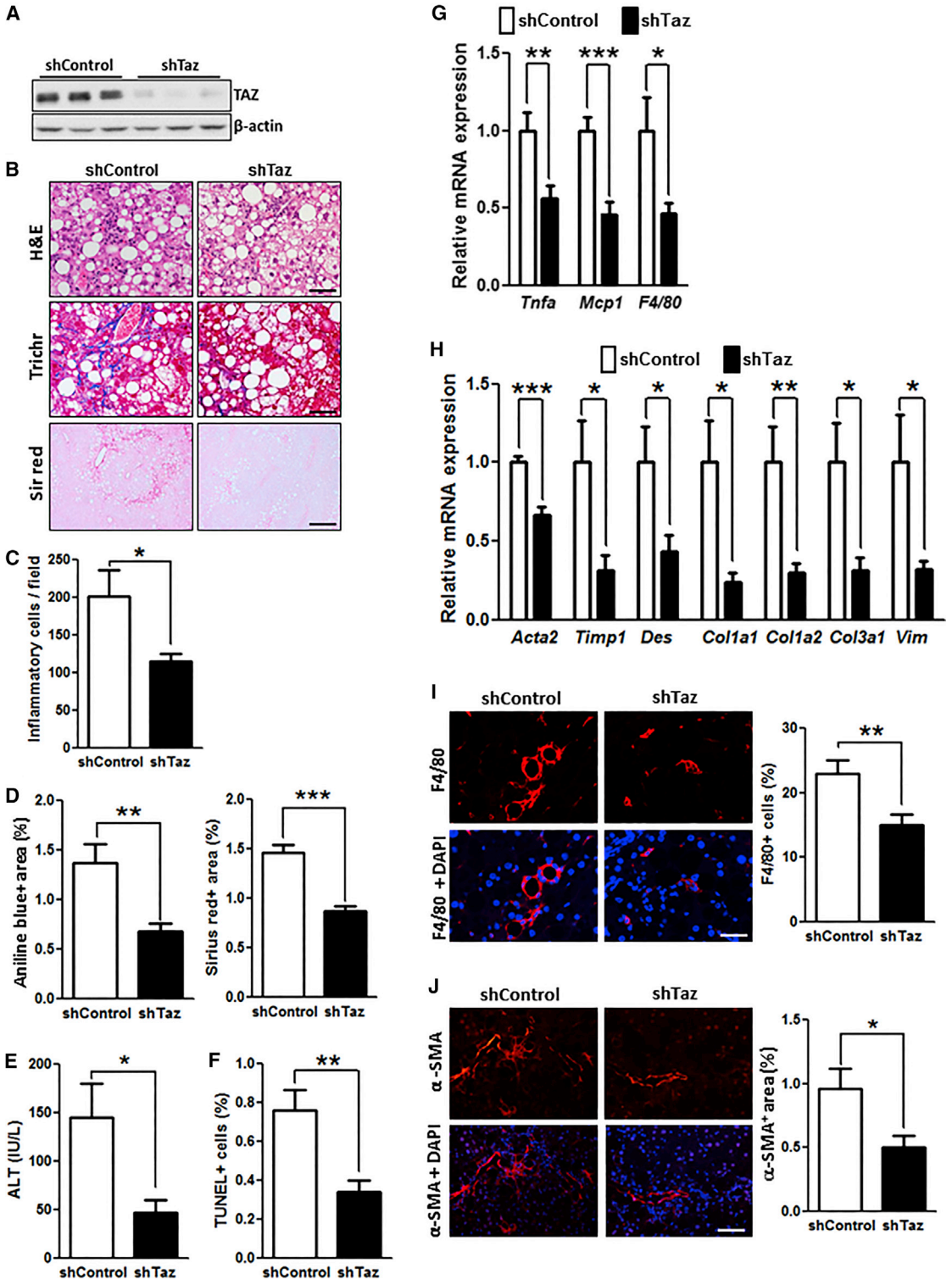

Figure 2. TAZ Silencing Reduces Liver Inflammation, Fibrosis, and Cell Death in FPC-Fed Mice

The following parameters were measured in male C57BL/6J mice treated with AAV8-H1-shTaz or control vector and then fed the FPC diet for 16 weeks (*$p < 0.05$, **$p < 0.01$, ***$p < 0.0002$, mean ± SEM; n = 10 mice/group):

(A) Immunoblot of TAZ in liver, with β-actin as loading control.

(B) Staining of liver sections for H&E (upper panels; bar, 100 μm), Masson's trichrome (Trichr) (middle panels; bar, 100 μm), and Sirius red (Sir red) (lower panels; bar, 500 μm).

(C) Hepatic inflammatory cells.

(legend continued on next page)

that TAZ is downstream of liver cholesterol accumulation (Figure S5M).

We conducted a similar study in which hyperphagic *Mc4r*$^{-/-}$ mice (Butler and Cone, 2002) were fed the FPC diet for 16 weeks. These mice develop more liver fibrosis compared with FPC-fed wild-type (WT) C57BL/6J mice, and silencing of Taz in the liver of these mice resulted in decreased staining for aniline blue, Sirius red, and α-SMA; lower hydroxyproline content; and decreased liver inflammation (Figure S6). We confirmed these results in the MCD model, where AAV8-H1-shTaz decreased both hepatic inflammation and fibrosis without affecting steatosis and also reduced inflammatory and fibrotic gene expression, α-SMA$^+$ cells, and macrophages in the liver (Figures S7A–S7J). In contrast, in a model of liver fibrosis in which TAZ is not increased in the liver—CCl4-treated mice—silencing Taz did not suppress fibrosis or fibrotic gene expression (Figures S7K–S7M). We also conducted an experiment in MCD-fed *Wwtr1*$^{fl/fl}$ mice (Xin et al., 2013) treated with AAV8-TBG-LacZ control or AAV8-TBG-Cre, which deletes floxed genes specifically in hepatocytes versus other types of liver cells (Mu et al., 2015) or other organs (Figures S8A and S8B). As above, inflammatory endpoints, α-SMA$^+$ cells, fibrosis-related gene expression, and cell death were decreased by hepatocyte TAZ knockdown, as was fibrosis itself, despite the fact that the level of fibrosis in the control cohort in this particular experiment was less than usual (Figures S8C–S8H).

We next asked whether features of NASH, notably fibrosis, could be reversed by treating mice with AAV8-H1-shTaz after NASH had developed. For this purpose, mice were placed on the FPC diet for 16 weeks, treated with shTaz or control vector, and then continued on the diet for an additional 12 weeks. As expected for 28 weeks of FPC feeding, the control mice had marked inflammation and fibrosis, and all parameters were decreased by Taz silencing (Figure 3). Thus, in separate models of NASH, hepatic TAZ silencing improved or reversed key liver parameters related to inflammation, fibrosis, and cell death without affecting metabolic parameters.

TAZ Silencing in Hepatocytes Blocks Steatosis-to-NASH Progression, and Genetically Induced TAZ Expression in Hepatocytes Promotes NASH in a Mouse Model of Steatosis

To investigate the role of TAZ specifically in steatosis-to-NASH progression, mice were first fed the FPC diet for 8 weeks and then injected with AAV8-H1-shTaz or control virus, followed by an additional 8 weeks on the diet. After 8 weeks, there was only a very slight increase in hepatic TAZ compared with mice fed the FPC diet for 16 weeks, and the livers showed steatosis but no appreciable inflammation or fibrosis (Figures 4A and 4B). The livers of mice who received shTaz at week 8 showed marked reductions at 16 weeks in fibrosis endpoints, inflammatory cells, inflammatory- and fibrosis-related genes, F4/80$^+$ macrophages, and α-SMA$^+$ cells, but not steatosis, and plasma ALT was also decreased by shTaz (Figures 4B–4H). These data suggest that TAZ is particularly important in the critical processes that promote steatosis-to-NASH progression.

Finally, whereas the above experiments addressed necessity of TAZ in NASH, we addressed the question of sufficiency by treating mice on the aforementioned FF diet, which is a model of steatosis in the time frame studied (above), with AAV8-albumin-TAZ. We achieved a level of hepatic TAZ protein in these mice that was similar to that in FPC-fed mice, and this was associated with an increase in all parameters of inflammation and fibrosis (Figure S9). Thus, TAZ is both necessary and sufficient to promote the development of NASH in mice.

Hepatocyte TAZ Induces Indian Hedgehog, which Promotes the Expression of Pro-Fibrotic Genes in Hepatic Stellate Cells and Mediates TAZ-Induced NASH

We sought to explore possible mechanisms linking TAZ to fibrosis progression. Previous studies have demonstrated that HSCs, the main source of collagen-producing myofibroblasts in NASH-related fibrosis (Mederacke et al., 2013), can be activated by the hedgehog pathway (Angulo et al., 2015b). In this context, chromatin immunoprecipitation (ChIP) array data suggested that the gene encoding Indian hedgehog, *Ihh*, is a TAZ/TEAD target. We therefore considered the hypothesis that increased TAZ in hepatocytes during NAFLD progression leads to the secretion of Ihh, which then acts on HSCs to promote the expression of pro-fibrotic genes.

To begin, we conducted TAZ ChIP analysis of livers of chow-fed and FPC-fed mice with or without TAZ silencing, focusing on a TAZ/TEAD consensus sequence in intron 1 of murine *Ihh* that is conserved among species, including humans (Zanconato et al., 2015) (Figures 5A and 5B). The results show a significant increase in the ChIP signal in the livers of FPC-fed versus chow-fed mice, which was dependent on anti-TAZ and was not seen when a non-consensus sequence was amplified. Most importantly, the ChIP signal in the livers of FPC mice was lowered to the chow level by TAZ silencing. Next, we conducted a dual-luciferase reporter assay using this intron 1 consensus sequence versus a mutated sequence, with 500 bp of upstream and downstream flanking sequence. The luciferase vectors were transfected into siControl- or siTaz-treated AML12 cells, a non-cancerous mouse hepatocyte cell line (Dumenco et al., 1995). The data showed robust luciferase activity with the consensus sequence versus mutated sequence in control AML12 cells, with a marked decrease in siTaz-treated cells (Figure 5C). Thus, TAZ interacts with a TAZ/TEAD consensus sequence in intron 1 of *Ihh* in the livers of FPC-fed mice, and this sequence can drive gene expression in a TAZ-dependent manner.

We next asked whether human NASH liver expressed higher levels of Ihh than normal and steatotic liver. As was the case

(D) Aniline blue- and Sirius red-positive area.
(E) Plasma ALT.
(F) TUNEL$^+$ cells.
(G) mRNA levels of *Tnfa*, *Mcp1*, and *F4/80* (*Adgre1*).
(H) mRNA levels of the indicated genes related to fibrosis.
(I) F4/80 immunofluorescence (red) and quantification; DAPI counterstain for nuclei is shown in bottom panels; bar, 100 μm.
(J) α-SMA immunofluorescence (red) and quantification; DAPI counterstain for nuclei is shown in bottom panels; bar, 100 μm.

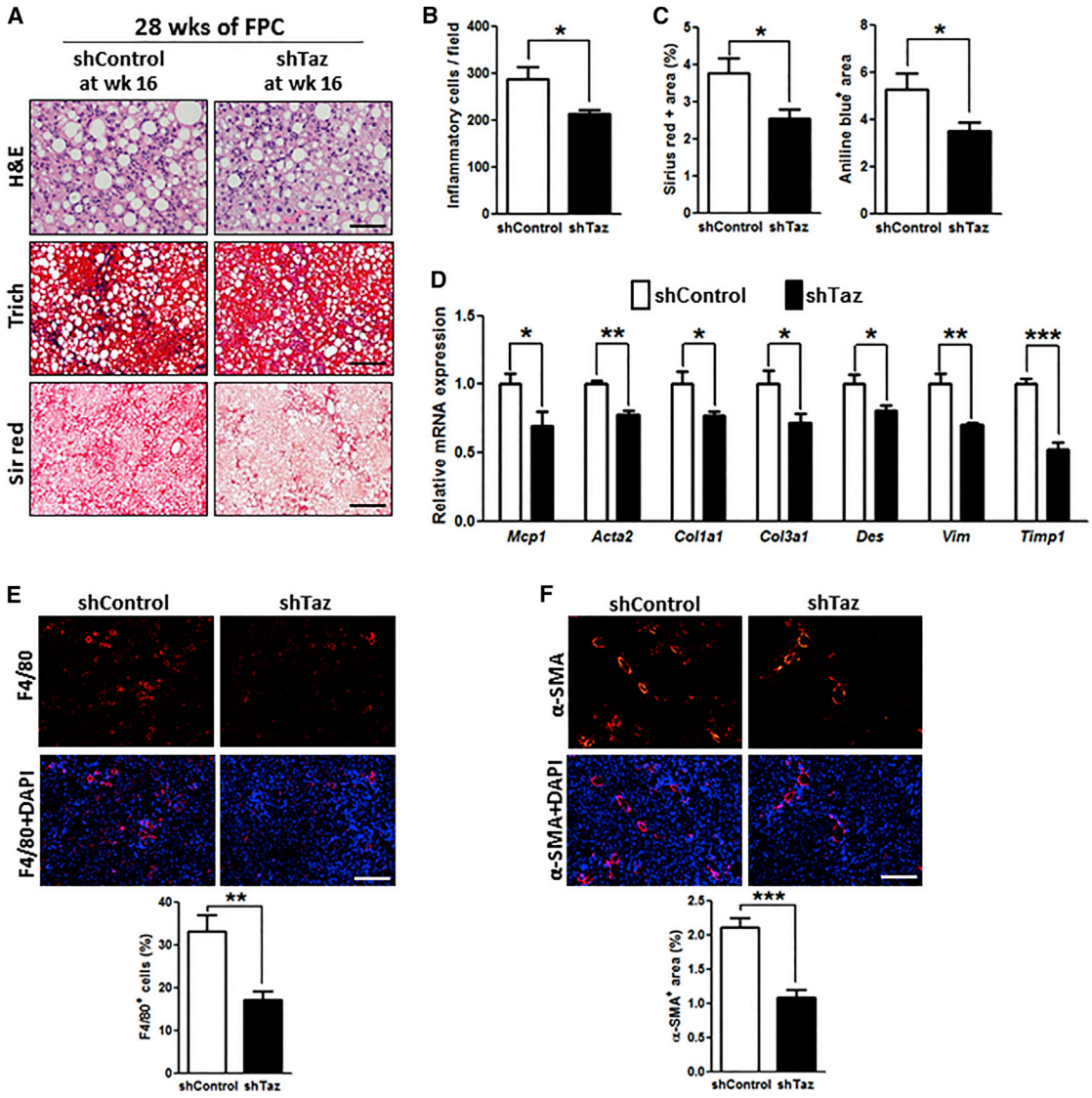

Figure 3. TAZ Silencing after the Development of NASH Reduces Liver Inflammation and Fibrosis in FPC-Fed Mice

The following parameters were measured in male C57BL/6J mice fed the FPC diet for 28 weeks, with AAV8-H1-shTaz or control vector administered at the 16 week time point (*$p < 0.05$; **$p < 0.01$, ***$p < 0.0001$, mean ± SEM; n = 5 mice/group):

(A) Staining of liver sections for H&E (upper panels; bar, 100 μm), Masson's trichrome (Trichr) (middle panels; bar, 500 μm), and Sirius red (Sir red) (lower panels; bar, 500 μm).

(B) Hepatic inflammatory cells.

(C) Aniline blue- and Sirius red-positive area.

(D) mRNA levels of *Mcp1*, *Acta2* (α-SMA), *Col1a1*, *Col3a1*, *Des*, *Vim*, and *Timp1*.

(E) F4/80 immunofluorescence (red) and quantification; DAPI counterstain for nuclei is shown in bottom panels; bar, 500 μm.

(F) α-SMA immunofluorescence (red) and quantification; DAPI counterstain for nuclei is shown in bottom panels; bar, 500 μm.

with TAZ (above), the expression of Ihh was greater in NASH liver than in normal and steatotic liver (Figure 5D). Similarly, the livers of FPC-fed mice had markedly higher levels of Ihh compared with the livers of chow-fed mice (Figure 5E). We then compared chow and FPC liver extracts for gene expression of *Ihh* and the Ihh pathway downstream genes Gli2 and Gli3. All three mRNAs were elevated in FPC liver, as was an Ihh target gene, osteopontin (*Opn*) (Razzaque et al., 2005), which is involved in HSC-induced fibrosis in NASH (Syn et al., 2011) (Figure 5F). To explore causation with regard to TAZ, we repeated these assays in FPC-fed mice with or without TAZ silencing. All four mRNAs and Ihh protein were substantially lower in the TAZ-silenced mice (Figures 5G and 5H), as was OPN as assessed by immunohistochemistry (Figure 5I). Thus, TAZ induces transcriptionally active Ihh during NASH progression in FPC-fed mice, and one of the targets of Ihh, *Opn*, has been linked to NASH fibrosis (Bohinc and Diehl, 2012; Syn et al., 2011).

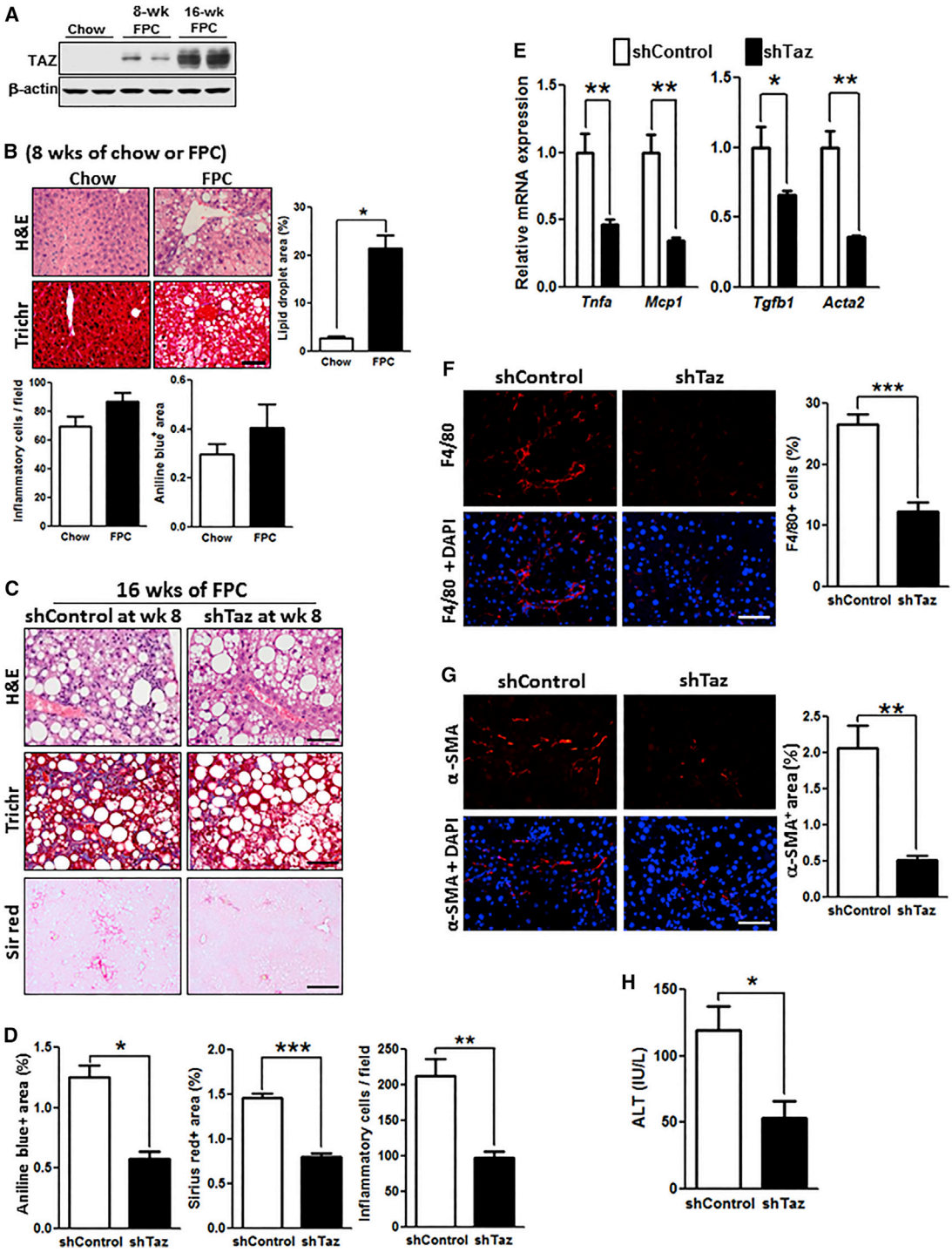

Figure 4. TAZ Silencing after the Development of Steatosis Reduces Liver Inflammation and Fibrosis in FPC-Fed Mice

(A) TAZ immunoblot of liver extracts from C57BL/6J mice fed chow or FPC diet for 8 or 16 weeks.

(B) H&E- and Masson's trichrome (Trich)-stained liver sections and quantified lipid droplet area, inflammatory cells, and aniline blue-positive area for C57BL/6J mice fed chow or FPC diet for 8 weeks. Bar, 100 μm.

(C–H) The following parameters were measured in male C57BL/6J mice fed the FPC diet for 16 weeks, with AAV8-H1-shTaz or control vector administered at the 8 week time point (*$p < 0.05$; **$p < 0.01$, ***$p < 0.0001$, mean ± SEM; n = 5 mice/group): staining of liver sections for H&E (upper panels; bar, 100 μm), Masson's trichrome (Trichr) (middle panels; bar, 100 μm), and Sirius red (Sir red) (lower panels; bar, 500 μm) (C); Aniline blue- and Sirius red-positive area and hepatic inflammatory cells (D); mRNA levels of *Tnfa*, *Mcp1*, *Tgfb1*, and *Acta2* (α-SMA) (E); F4/80 immunofluorescence (red) and quantification; DAPI counterstain for nuclei is shown in bottom panels; bar, 100 μm (F); α-SMA immunofluorescence (red) and quantification; DAPI counterstain for nuclei is shown in bottom panels; bar, 100 μm (G); and plasma ALT (H).

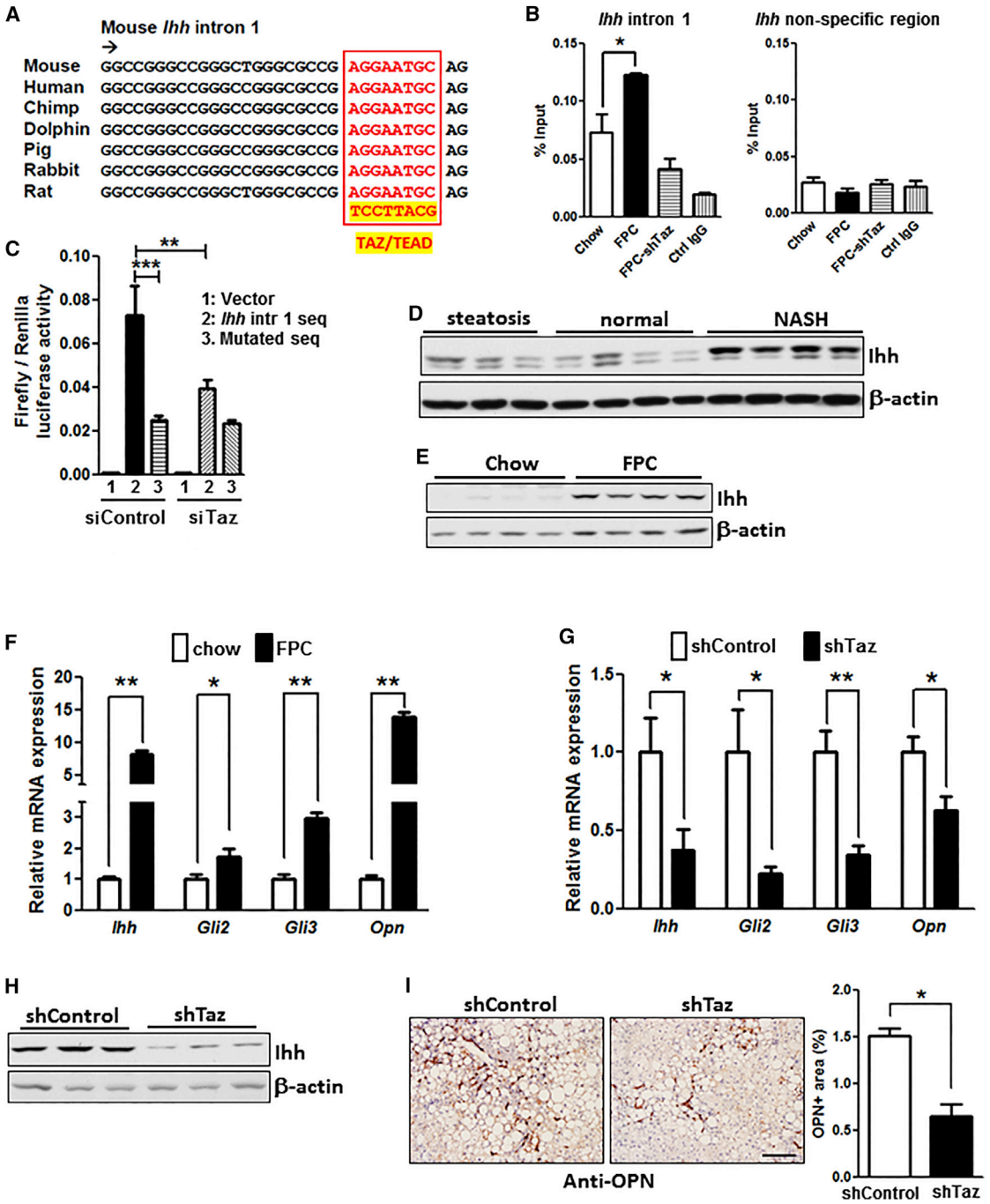

Figure 5. TAZ Induces *Ihh*, and TAZ Silencing Lowers the Expression of Pro-Fibrotic Hedgehog Pathway Genes in the Livers of FPC-Fed Mice

(A) Conserved TAZ/TEAD consensus sequence in intron 1 of the mouse *Ihh* gene.

(B) Liver nuclear extracts from mice fed chow diet or FPC diet for 16 weeks with or without TAZ silencing were subjected to TAZ ChIP analysis using anti-TAZ or IgG control. The intronic region containing the TAZ/TEAD binding sequence, or a non-consensus sequence as control, was amplified by qPCR and normalized to the values obtained from input DNA (*p = 0.03; mean ± SEM; n = 3).

(C) A dual-luciferase reporter assay in control and TAZ-silenced AML12 cells was conducted using the *Ihh* intron 1 region in (B), or a mutated version, together with 500 bp of flanking upstream and downstream sequence. (**p < 0.01, ***p < 0.0001; mean ± SEM; n = 6).

(D) Immunoblot of Ihh in normal human livers or those with steatosis or NASH.

(E) Immunoblot of Ihh in the livers of mice fed chow or FPC diet for 16 weeks.

(F) Relative expression of *Ihh*, *Gli2*, *Gli3*, and *Opn* mRNAs in the livers of mice fed chow or FPC diet for 16 weeks (*p < 0.04, **p < 0.0001; mean ± SEM; n = 6).

(legend continued on next page)

To explore the possibility that TAZ-induced Ihh is secreted by hepatocytes and activates HSCs, we moved to an in vitro model using both AML12 cells and primary murine HSCs. Consistent with our data in vivo, siTaz treatment of AML12 cells lowered cellular *Ihh* mRNA in the cells and Ihh protein in both the cells and media (Figures 6A–6C). We then added conditioned medium (CM) from control or Taz-silenced AML12 cells, as well as medium not exposed to cells (non-CM), to primary murine HSCs. Compared with non-CM, hepatocyte CM markedly increased *Opn* mRNA as well as the mRNAs for two proteins involved in fibrosis, *Timp1* and *Col1a1*. Most importantly, CM from TAZ-silenced hepatocytes lowered the levels these mRNAs and protein compared to CM from control hepatocytes (Figure 6D). Conditioned medium from *Ihh*-silenced hepatocytes also decreased the three mRNAs in HSCs (Figure 6E), although the absolute degree of *Timp1* lowering was somewhat greater in this experiment than in the siTaz experiment. Finally, to make a more direct link between TAZ-induced Ihh in hepatocytes and activation of HSCs, we restored Ihh in siTaz-treated hepatocytes by Ihh transfection and then asked whether this lessened the suppressive effect of CM from these cells on the expression of the fibrosis-related genes in HSCs. Transfection of TAZ-silenced hepatocytes with Ihh led to a level of Ihh in the CM that was similar to that in the CM of control hepatocytes (Figure 6F—compare first and fourth bars). As before, the CM of TAZ-silenced hepatocytes suppressed *Opn*, *Timp1*, and *Col1a1* mRNA in HSCs (Figure 6G—compare second and fourth bars), and we found that restoration of *Ihh* in these TAZ-silenced cells rescued CM-induced HSC gene expression (Figure 6G—compare fourth and fifth bars). Finally, we wondered whether TAZ might also directly regulate fibrogenic gene expression or proliferation in HSCs. However, we found that silencing of Taz in primary HSCs affected neither fibrogenic gene expression nor cell proliferation (Figure 6H). Together, these studies suggest that hepatocyte-induced Ihh in hepatocytes promotes the expression of pro-fibrotic genes in HSCs.

To provide causation evidence in vivo for the role Ihh in TAZ-induced NASH, we first used AAV8-*Ihh* to restore Ihh in *Taz*-silenced FPC-fed mice. As designed, the level of hepatic *Ihh* mRNA in Ihh-restored shTaz mice was similar to that in control mice (Figure 7A, first set of bars). Consistent with the TAZ-Ihh hypothesis, Ihh restoration prevented the improvement in all NASH features that we see with Taz silencing, including liver inflammation, fibrosis and fibrogenic mRNA expression, and cell death (Figures 7A–7D). Next, we directly silenced Ihh in FPC-fed mice using AAV8-H1-sh*Ihh* and found that this intervention, like silencing Taz, improved all NASH-like features (Figures 7E–7L). These combined in vitro and in vivo data support the conclusion that hepatocyte TAZ promotes NASH progression in large part through inducing Ihh.

DISCUSSION

NASH, characterized by inflammation, cell death, and fibrosis, can progress to advanced liver disease, cirrhosis, and the need for liver transplant. Steatosis alone is believed to be little to no risk for progressive liver disease. Given the clinical significance of NASH compared to steatosis (Rinella, 2015), a critical objective of research in this area is to identify factors and pathways that promote the conversion of steatosis to NASH and the development of fibrosis. The importance of this objective is underscored by the fact that NASH is becoming the leading cause of liver disease worldwide and yet lacks any definitive, evidence-based drug therapies approved by the US Food and Drug Administration (Rinella, 2015). In this context, the finding that a hepatocyte TAZ-Ihh pathway plays a key role in steatosis-to-NASH conversion and the development of fibrosis provides new insight into NASH and may suggest new targets for therapy.

Hepatic fibrosis is a key feature of NASH that distinguishes it from steatosis and determines long-term mortality in patients with NASH (Angulo et al., 2015a). While both TAZ and YAP have been implicated in organ fibrosis in other settings, particularly in the lung with links to TGFβ-SMAD signaling or induction of plasminogen activator inhibitor-1 (Liu et al., 2015; Mitani et al., 2009; Piersma et al., 2015; Saito and Nagase, 2015), there are only scattered reports about their roles in liver fibrosis and none in the setting of NAFLD. For example, a recent study reported an association between microRNA-130/301, which can regulate TAZ and YAP, and CCl_4-induced liver fibrosis (Bertero et al., 2015), but there were no direct causation or mechanistic data related to the role of TAZ in this process, and we now show that TAZ is not involved in CCl_4-induced liver fibrosis. Another report showed that knockout of a pair of Hippo factors called Mps One Binder Kinase Activator (MOB)1A/1B in lean, non-NASH mice caused elevated TGFβ-2/3 and liver fibrosis in a manner that was partially dependent on TAZ (Nishio et al., 2016).

Although the mechanism of TAZ in liver fibrosis in NASH is likely to be multifactorial, we show here that the TAZ target Ihh is elevated in human and mouse NASH liver in a TAZ-dependent manner and is important in NASH progression and fibrosis. Previous work has implicated hedgehog signaling in NASH fibrosis, particularly *Shh* signaling in HSCs (Bohinc and Diehl, 2012), both directly and via the induction of the pro-fibrotic cytokine IL-13 by immune cells (Shimamura et al., 2008; Syn et al., 2010). ChIP array data (Zhao et al., 2008) suggested to us that *Ihh* might be a TAZ/TEAD target gene by interacting with a consensus site in intron 1 of the *Ihh* gene, which we have now confirmed using complementary ChIP and luciferase reporter assays. Most importantly, hepatocyte TAZ-induced *Ihh* activated a fibrosis program in HSCs in cell culture, restoration of Ihh in hepatocyte-TAZ-silenced mice restored NASH progression, and direct silencing Ihh in hepatocytes suppressed NASH.

(G) Relative expression of *Ihh*, *Gli2*, *Gli3*, and *Opn* mRNAs in the livers of mice fed the FPC diet for 16 weeks with or without TAZ silencing (*$p < 0.05$, **$p < 0.002$; mean ± SEM; n = 10).

(H) Immunoblot of Ihh in the livers of mice fed the FPC diet for 16 weeks with or without TAZ silencing.

(I) OPN immunohistochemistry and quantification in the livers of mice fed the FPC diet for 16 weeks with or without TAZ silencing (*$p < 0.0001$; mean ± SEM; n = 10); bar, 200 μm.

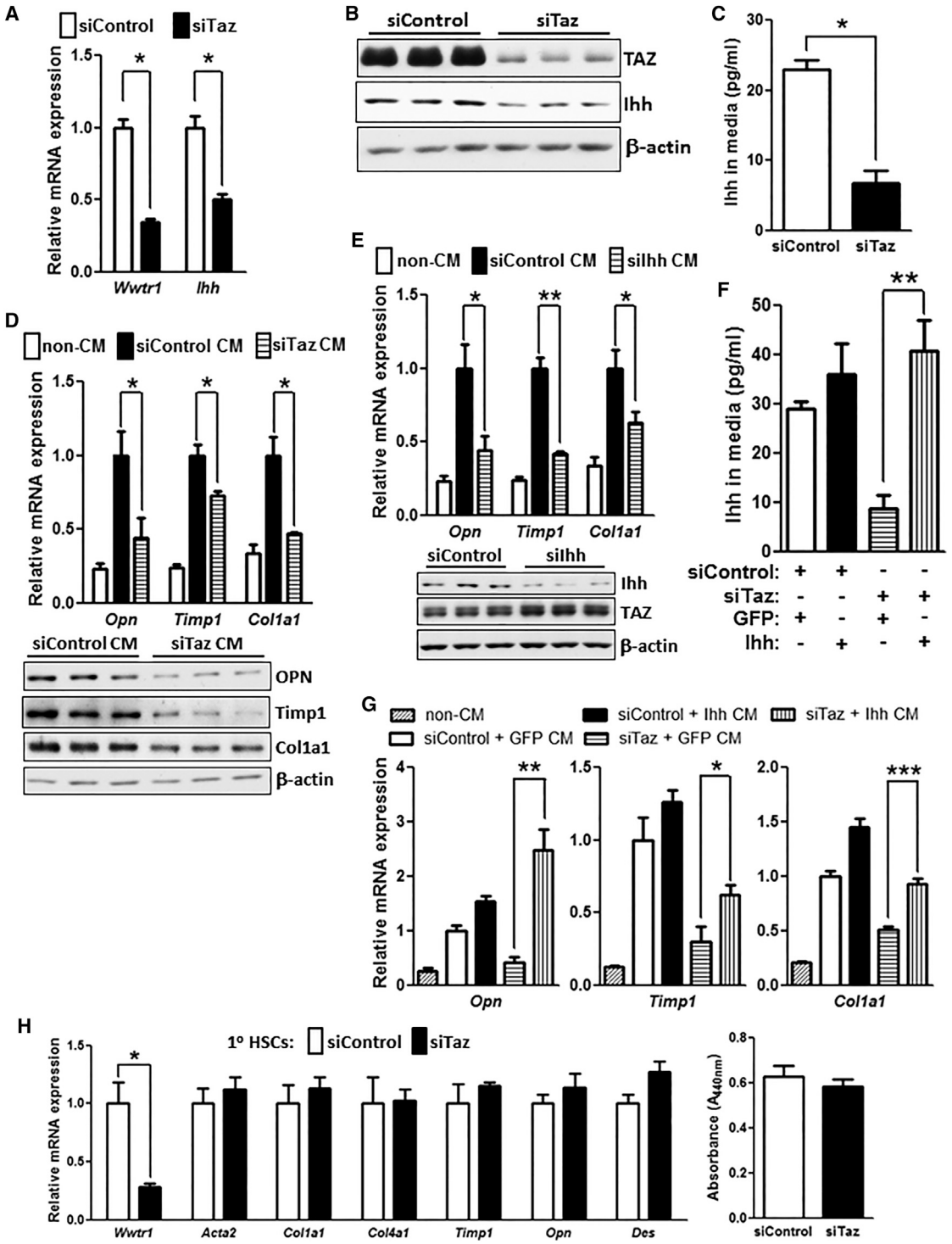

Figure 6. TAZ-Induced Hepatocyte Ihh Increases the Expression of Fibrosis-Related Genes in Hepatic Stellate Cells

(A) Expression of *Wwtr1* and *Ihh* mRNA in control and TAZ-silenced AML12 cells (*p < 0.0003; mean ± SEM; n = 3).

(B) Immunoblot of TAZ and Ihh in control and TAZ-silenced AML12 cells.

(C) Ihh concentrations, assayed by ELISA, in the media of control and TAZ-silenced AML12 cells (*p < 0.003; mean ± SEM; n = 3).

(D) Primary hepatic stellate cells (HSCs) were incubated for 72 hr with conditioned medium (CM) obtained from control or Taz-silenced AML12 cells or with medium not exposed to cells (non-CM). The HSCs were then assayed for *Opn*, *Timp1*, and *Col1a1* mRNA (upper panel; *p < 0.05; mean ± SEM; n = 4) and the respective proteins by immunoblot (lower panel).

(legend continued on next page)

Two other critical features of NASH, inflammation and cell death, were also ameliorated by TAZ silencing in our study. Little is known about the pro-inflammatory roles of TAZ, and, in general, YAP and TAZ inhibit, rather than promote, apoptosis during development and in cancer (Yu et al., 2015). However, there is one report showing that siTaz decreased TNFα-induced apoptosis in salivary gland epithelial cells (Hwang et al., 2014). RIP3-mediated necroptosis may also be important in hepatocyte death in NASH (Gautheron et al., 2014), and therefore it is possible that TAZ promotes this pathway. Given the various consequences of cell necrosis, this action of TAZ could contribute to inflammation and fibrosis, as well as cell death, in NASH (Chan et al., 2015; Luedde et al., 2014).

Our study focused on TAZ in hepatocytes, but a recent report showed that YAP was significantly increased in progenitor-like reactive-appearing ductular cells (RDCs) in human and mouse NASH liver (Machado et al., 2015). We also found increased YAP in the livers of FPC mice, and consistent with the data of Machado et al., most of the YAP-positive cells did not co-localize with HNF4α-positive hepatocytes (data not shown). While the role of YAP in NASH remains to be elucidated, the authors showed correlations among YAP^+ RDCs, fibrosis, accumulation of myofibroblasts, and expression of *Shh* and *Opn*. Of note, silencing TAZ in the livers of FPC mice did not affect YAP expression (data not shown).

Most of our experiments were conducted in a mouse model of insulin resistance and NAFLD that was a modification of previously described models (Charlton et al., 2011; Kohli et al., 2010). The diet was based on human dietary risk factors for NASH, and the key improvement over previous models was the development of inflammation, hepatocyte death, and fibrosis in 16 weeks without the need for genetically engineered mutations and in the background of weight gain and insulin resistance. Whereas the fructose component of the diet likely contributes to steatosis (Abdelmalek et al., 2010; Ishimoto et al., 2013), the cholesterol and palmitic acid components may be important in NASH progression and perhaps TAZ induction. The accumulation of unesterified cholesterol in the liver has been implicated in the development of NASH in humans (Ioannou, 2016) and in various mouse models (Subramanian et al., 2011; Van Rooyen et al., 2011; Wouters et al., 2008). For example, studies using mice fed high-cholesterol diets have suggested that cholesterol can directly activate HSCs by inducing TLR4, promote oxidative stress and cell death in hepatocytes via excess mitochondrial cholesterol, and promote inflammation in Kupffer cells through lysosomal cholesterol enrichment (Bieghs et al., 2013; Rawson, 2006; Teratani et al., 2012). If increased liver cholesterol is important in TAZ induction in NASH, further studies will be needed to define the mechanisms. Likewise, palmitic acid has been reported to induce pro-inflammatory cytokine production by hepatocytes and Kupffer cells during NASH (Joshi-Barve et al., 2007; Miura et al., 2013), but other mechanisms may be involved as well.

In summary, we show that the Hippo pathway transcription factor TAZ and its gene target Ihh are elevated in the livers of humans with NASH, which is recapitulated in mouse models. In these models, silencing of TAZ or Ihh suppresses key features of NASH progression, but not steatosis. Moreover, silencing TAZ after NASH has developed can partially reverse NASH features, including fibrosis. Although further mechanistic work is needed to fully understand these new findings, the data provide new insight into the pathophysiology of NASH and raise the possibility of liver-directed TAZ inhibition as a new therapeutic strategy to prevent NASH progression.

EXPERIMENTAL PROCEDURES

Animal Studies

Male wild-type mice C57BL/6J (#000664, 8–10 weeks old) and MC4R-negative *loxTB Mc4r* mice (#006414, 6 weeks old), referred to here as $Mc4r^{-/-}$ mice, were obtained from Jackson Laboratory and were allowed to adapt to housing in the Columbia University Medical Center Institute of Comparative Medicine for 1 week prior to random assignment to experimental cohorts. $Wwtr1^{fl/fl}$ mice were generously provided by Dr. Eric Olson, University of Texas Southwestern. The mice were then fed the following diets for the times indicated in the figure legends: (1) chow diet (Picolab rodent diet 20, #5053); (2) "fast-food" (FF) diet (TestDiet 1810060): high-fat diet with drinking water containing 42 g/L glucose and fructose (55%/45%, w/w); or (3) fructose-palmitate-cholesterol ("FPC") diet (Teklad, TD.140154): similar to FF diet but with 1.25% added cholesterol and with palmitic acid, anhydrous milk fat, and Primex as the sources of fat and with an ~60% decrease in vitamin E and an ~35% decrease in choline compared with typical mouse diets. The detailed composition of these diets appear in Tables S1 and S2. For several experiments, groups of mice were placed on a methionine-choline-deficient diet (MCD Diet, Teklad, TD. 90262) for 8 weeks, as described (Dixon et al., 2012). AAV8-TBG-Cre or control AAV8-TBG-LacZ (1×10^{11} genome copies/mouse) was administered to $Wwtr1^{fl/fl}$ mice by tail vein injection 1 week prior to initiation of the MCD diet. AAV8-H1 shRNA virus or control AAV8-H1 virus (2×10^{11} genome copies/mouse) was delivered by tail vein injection either 1 week prior to FPC diet initiation or after 8 or 16 weeks of the diet. For CCl_4-induced liver fibrosis, 6-week-old C57BL/6J mice were injected intraperitoneally (i.p.) biweekly for 6 weeks with 0.5 μL/g body weight of CCl_4, which was dissolved in olive oil at a ratio of 1:3 (Mederacke et al., 2013). For the imaging of organs undergoing AAV8-TBG-Cre-mediated recombination, ZsGreen reporter mice (#007906, Jackson Laboratory) (Mu et al., 2015) were injected intravenously (i.v.) with AAV8-TBG-Cre (1×10^{11} genome copies/mouse). 1 week later, the mice were sacrificed, and selected organs were fixed and then imaged using a Leica MZ 16F fluorescence stereomicroscope. Animals were housed in standard cages at 22°C in a 12 hr light/12 hr dark cycle. All animal experiments were performed in accordance with institutional guidelines and regulations and approved by the Institutional Animal Care and Use Committee at Columbia University.

(E) HSCs were incubated for 72 hr with non-CM or CM obtained from control or Ihh-silenced AML12 cells and then assayed for *Opn*, *Timp1*, and *Col1a1* mRNA (*$p < 0.04$; **$p < 0.0001$, mean ± SEM; n = 4). Immunoblot of Ihh and TAZ in siIhh-treated and control AML12 cells is shown below the graph.

(F) Control or Taz-silenced AML12 cells that were transduced with a plasmid encoding Ihh or control GFP. Aliquots of the four sets of conditioned medium were assayed for Ihh by ELISA (*$p < 0.002$; mean ± SEM; n = 3).

(G) HSCs were incubated with conditioned media from the four sets of cells in (F) or with non-CM and then assayed for *Opn*, *Timp1*, and *Col1a1* mRNA (*$p < 0.05$; **$p < 0.004$, ***$p < 0.0004$, mean ± SEM; n = 4). Note that bars 2 and 3 for *Opn* and *Col1a1* are significantly different at $p < 0.05$.

(H) Primary HSCs were activated by culturing for 72 hr in medium containing 10% FBS and then treated with siControl or siTaz duplex, followed by culturing in the same medium for an additional 48 hr. The cells were then assayed for *Wwtr1*, *Acta2*, *Col1a1*, *Col4a1*, *Timp1*, *Opn*, and *Des* mRNAs or cell proliferation. For the proliferation assay, the cells were synchronized by overnight culture in medium containing 0.2% FBS and then cultured an additional 48 hr in medium containing 10% FBS. The cells were incubated with WST-1, and absorbance at 440 nm was measured to assess cell number.

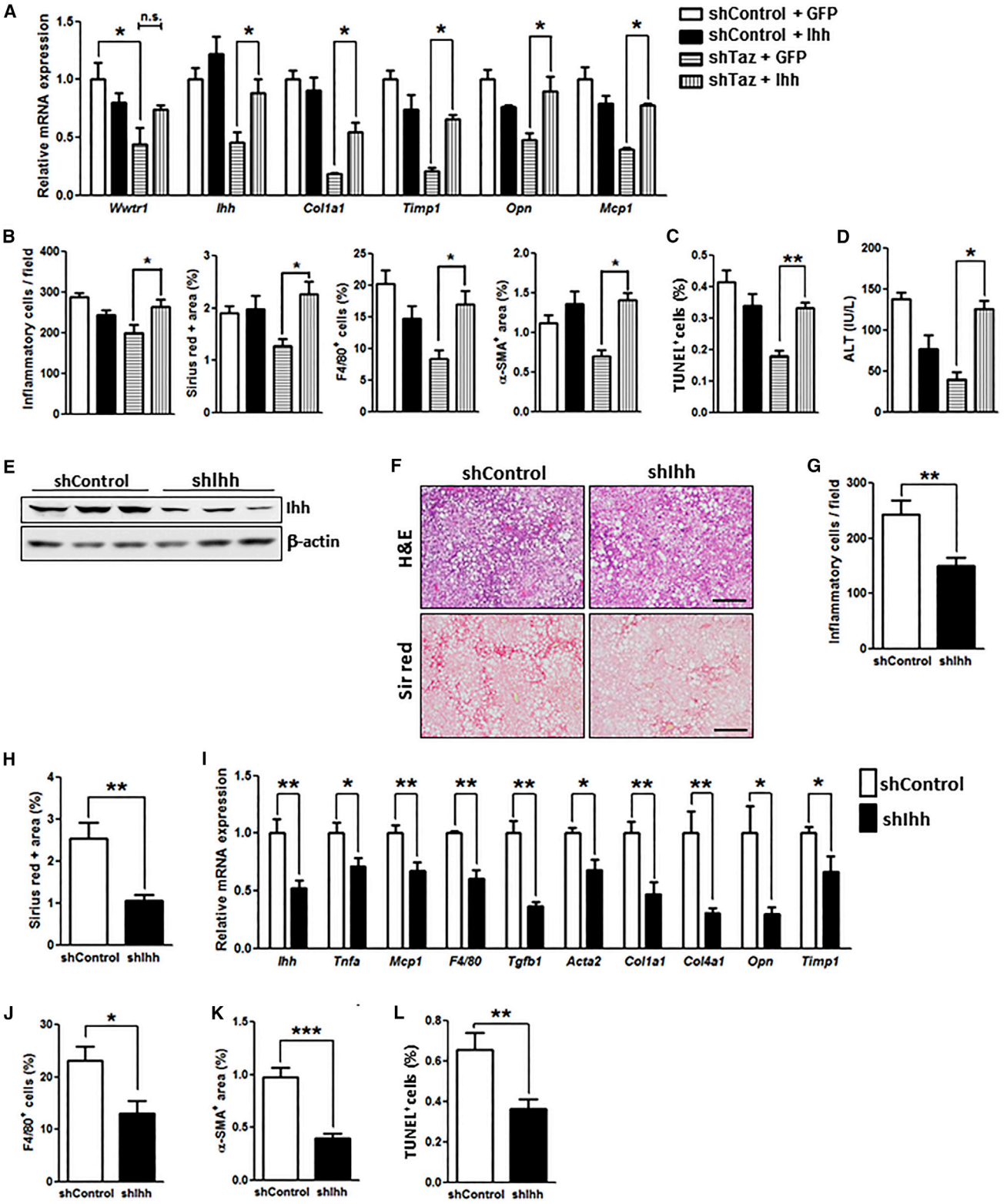

Figure 7. Ihh Restoration in Taz-Silenced FPC-Fed Mice Promotes NASH Features, and Ihh Silencing Reduces NASH Features

(A–D) The following parameters were measured in male C57BL/6J mice treated with AAV8-H1-shTaz or control vector and then overexpressed Ihh or GFP by AAV8 vector and fed the FPC diet for 16 weeks (*$p < 0.05$, **$p < 0.01$, mean ± SEM; n = 6 mice/group): mRNA levels of *Wwtr1*, *Ihh*, *Col1a1*, *Timp1*, *Opn*, and *Mcp1* (A); quantification of inflammatory cells, Sirius red positive area, F4/80$^+$ cells, and α-SMA$^+$ area (B); TUNEL$^+$ cells (C); and plasma ALT (D).

(legend continued on next page)

Human Samples

Liver biopsy specimens from individuals undergoing weight loss surgery were selected from the MGH NAFLD Biorepository. Patients gave informed consent at the time of recruitment, and their records were anonymized and de-identified. Studies were approved by the Columbia University Institutional Review Board and by the Partners Human Research Committee and conducted in accordance with National Institutes of Health and institutional guidelines for human subject research. Additional anonymized and de-identified liver biopsy sections were obtained from Dr. Jay Lefkowitch, Columbia University Medical Center. Cases with NAFLD activity score of 1–3 were classified as early NAFLD (no fibrosis), while cases with NAS $\geq$ 5 and fibrosis stage 1a/b-4 were classified as NASH. Cases with steatosis score $\geq$1 and inflammation and ballooning scores of 0 and no fibrosis were classified as steatosis. Cases with NAS 0 were classified as normal.

Blood and Plasma Analyses

Fasting blood glucose was measured using a glucose meter (One Touch Ultra, LifeScan) in mice that were fasted for 4–5 hr with free access to water. Complete blood counts were obtained with the FORCYTE Veterinary Hematology Analyzer (Oxford Science). Total plasma triglyceride and cholesterol were assayed using a commercially available kit from Wako. For insulin, MCP1, AST, ALT, TC, and TG are measured following kit instruction by using plasma.

Statistical Analysis

All results are presented as mean ± SEM. p values were calculated using the Student's t test for normally distributed data and the Mann-Whitney rank sum test for non-normally distributed data. One-way ANOVA with post hoc Tukey test was used to evaluate differences among groups when three or more groups were analyzed.

SUPPLEMENTAL INFORMATION

Supplemental Information includes Supplemental Experimental Procedures, nine figures, and four tables and can be found with this article online at http://dx.doi.org/10.1016/j.cmet.2016.09.016.

AUTHOR CONTRIBUTIONS

X.W., R.F.S., and I.T. developed the study concept and experimental design; X.W. performed all animal study procedures and most of the in vitro experiments; Z.Z. conducted the ChIP assays; J.M.C. conducted the fluorescence reporter mouse assay, hydroxyproline measurements, and αSMA IHC experiments. B.C. conducted the CCl_4-induced liver fibrosis experiment. K.E.C., R.C., and J.H.L. collected and helped analyze the human samples; T.M.H. helped design the FPC diet; R.M. scored mouse liver for NASH features; and X.W., R.F.S., and I.T. interpreted the data and wrote the manuscript.

ACKNOWLEDGMENTS

We thank Dr. Utpal Pajvani, Columbia University, for helpful discussions; Dr. Yuri Choi, Massachusetts General Hospital, for assisting with the human liver samples; Dr. Stephen M. Lagana, Columbia University, for human NASH liver histology analysis; Dr. Rhonda Bassel-Duby and Dr. Eric Olson, UT Southwestern, for sharing *Wwtr1*$^{fl/fl}$ mice; Dr. Hongfeng Jiang, Columbia University, for conducting the liver lipid profiling experiment; and Dr. Peter Nagy, Columbia University, for assisting with the ChIP experiments. This work was supported by NIH grants HL087123 and HL075662 to I.T.; DK078772 to R.T.C.; DK99422 to K.E.C.; and R03DK101863 to J.M.C. Z.Z. is a Russell Berrie Foundation Scholar in Diabetes Research. R.M. is supported by a Pinnacle Research Award from the AASLD Foundation. B.C. is supported by an American Heart Association Post-Doctoral Fellowship. The liver lipid profiling work was supported by NIH Grant Number UL1 TR000040 from the National Center for Advancing Translational Science.

Received: March 17, 2016
Revised: August 6, 2016
Accepted: September 24, 2016
Published: October 27, 2016

REFERENCES

Abdelmalek, M.F., Suzuki, A., Guy, C., Unalp-Arida, A., Colvin, R., Johnson, R.J., and Diehl, A.M.; Nonalcoholic Steatohepatitis Clinical Research Network (2010). Increased fructose consumption is associated with fibrosis severity in patients with nonalcoholic fatty liver disease. Hepatology *51*, 1961–1971.

Angulo, P., Kleiner, D.E., Dam-Larsen, S., Adams, L.A., Bjornsson, E.S., Charatcharoenwitthaya, P., Mills, P.R., Keach, J.C., Lafferty, H.D., Stahler, A., et al. (2015a). Liver fibrosis, but no other histologic features, is associated with long-term outcomes of patients with nonalcoholic fatty liver disease. Gastroenterology *149*, 389–397.e10.

Angulo, P., Machado, M.V., and Diehl, A.M. (2015b). Fibrosis in nonalcoholic fatty liver disease: mechanisms and clinical implications. Semin. Liver Dis. *35*, 132–145.

Bertero, T., Cottrill, K.A., Annis, S., Bhat, B., Gochuico, B.R., Osorio, J.C., Rosas, I., Haley, K.J., Corey, K.E., Chung, R.T., et al. (2015). A YAP/TAZ-miR-130/301 molecular circuit exerts systems-level control of fibrosis in a network of human diseases and physiologic conditions. Sci. Rep. *5*, 18277.

Bieghs, V., Hendrikx, T., van Gorp, P.J., Verheyen, F., Guichot, Y.D., Walenbergh, S.M., Jeurissen, M.L., Gijbels, M., Rensen, S.S., Bast, A., et al. (2013). The cholesterol derivative 27-hydroxycholesterol reduces steatohepatitis in mice. Gastroenterology *144*, 167–178.e1.

Bohinc, B.N., and Diehl, A.M. (2012). Mechanisms of disease progression in NASH: new paradigms. Clin. Liver Dis. *16*, 549–565.

Butler, A.A., and Cone, R.D. (2002). The melanocortin receptors: lessons from knockout models. Neuropeptides *36*, 77–84.

Chan, F.K., Luz, N.F., and Moriwaki, K. (2015). Programmed necrosis in the cross talk of cell death and inflammation. Annu. Rev. Immunol. *33*, 79–106.

Charlton, M., Krishnan, A., Viker, K., Sanderson, S., Cazanave, S., McConico, A., Masuoko, H., and Gores, G. (2011). Fast food diet mouse: novel small animal model of NASH with ballooning, progressive fibrosis, and high physiological fidelity to the human condition. Am. J. Physiol. Gastrointest. Liver Physiol. *301*, G825–G834.

Corey, K.E., and Kaplan, L.M. (2014). Obesity and liver disease: the epidemic of the twenty-first century. Clin. Liver Dis. *18*, 1–18.

Day, C.P., and James, O.F. (1998). Steatohepatitis: a tale of two "hits"? Gastroenterology *114*, 842–845.

Dixon, L.J., Berk, M., Thapaliya, S., Papouchado, B.G., and Feldstein, A.E. (2012). Caspase-1-mediated regulation of fibrogenesis in diet-induced steatohepatitis. Lab. Invest. *92*, 713–723.

Dumenco, L., Oguey, D., Wu, J., Messier, N., and Fausto, N. (1995). Introduction of a murine p53 mutation corresponding to human codon 249 into a murine hepatocyte cell line results in growth advantage, but not in transformation. Hepatology *22*, 1279–1288.

Friedman, S.L. (2008). Mechanisms of hepatic fibrogenesis. Gastroenterology *134*, 1655–1669.

Gautheron, J., Vucur, M., Reisinger, F., Cardenas, D.V., Roderburg, C., Koppe, C., Kreggenwinkel, K., Schneider, A.T., Bartneck, M., Neumann, U.P., et al.

(E–L) The following parameters were measured in male C57BL/6J mice treated with AAV8-H1-sh*Ihh* or control vector and then fed the FPC diet for 16 weeks (*p < 0.05, **p < 0.01, ***p < 0.0001, mean ± SEM; n = 5 mice/group): immunoblot of Ihh, with β-actin as loading control (E); staining of liver sections for H&E (upper panels; bar, 500 μm) and Sirius red (Sir red) (lower panels; bar, 500 μm) (F); hepatic inflammatory cells (G); Sirius red-positive area (H); mRNA levels of the indicated genes related to inflammation and fibrosis (I); F4/80$^+$ cells (J); α-SMA$^+$ area (K); and TUNEL$^+$ cells (L).

(2014). A positive feedback loop between RIP3 and JNK controls non-alcoholic steatohepatitis. EMBO Mol. Med. *6*, 1062–1074.

Hebbard, L., and George, J. (2011). Animal models of nonalcoholic fatty liver disease. Nat. Rev. Gastroenterol. Hepatol. *8*, 35–44.

Hwang, S.M., Jin, M., Shin, Y.H., Ki Choi, S., Namkoong, E., Kim, M., Park, M.Y., and Park, K. (2014). Role of LPA and the Hippo pathway on apoptosis in salivary gland epithelial cells. Exp. Mol. Med. *46*, e125.

Ioannou, G.N. (2016). The role of cholesterol in the pathogenesis of NASH. Trends Endocrinol. Metab. *27*, 84–95.

Ishimoto, T., Lanaspa, M.A., Rivard, C.J., Roncal-Jimenez, C.A., Orlicky, D.J., Cicerchi, C., McMahan, R.H., Abdelmalek, M.F., Rosen, H.R., Jackman, M.R., et al. (2013). High-fat and high-sucrose (western) diet induces steatohepatitis that is dependent on fructokinase. Hepatology *58*, 1632–1643.

Jolley, C.D., Dietschy, J.M., and Turley, S.D. (1999). Genetic differences in cholesterol absorption in 129/Sv and C57BL/6 mice: effect on cholesterol responsiveness. Am. J. Physiol. *276*, G1117–G1124.

Joshi-Barve, S., Barve, S.S., Amancherla, K., Gobejishvili, L., Hill, D., Cave, M., Hote, P., and McClain, C.J. (2007). Palmitic acid induces production of proinflammatory cytokine interleukin-8 from hepatocytes. Hepatology *46*, 823–830.

Kohli, R., Kirby, M., Xanthakos, S.A., Softic, S., Feldstein, A.E., Saxena, V., Tang, P.H., Miles, L., Miles, M.V., Balistreri, W.F., et al. (2010). High-fructose, medium chain trans fat diet induces liver fibrosis and elevates plasma coenzyme Q9 in a novel murine model of obesity and nonalcoholic steatohepatitis. Hepatology *52*, 934–944.

Lisowski, L., Dane, A.P., Chu, K., Zhang, Y., Cunningham, S.C., Wilson, E.M., Nygaard, S., Grompe, M., Alexander, I.E., and Kay, M.A. (2014). Selection and evaluation of clinically relevant AAV variants in a xenograft liver model. Nature *506*, 382–386.

Liu, C.Y., Lv, X., Li, T., Xu, Y., Zhou, X., Zhao, S., Xiong, Y., Lei, Q.Y., and Guan, K.L. (2011). PP1 cooperates with ASPP2 to dephosphorylate and activate TAZ. J. Biol. Chem. *286*, 5558–5566.

Liu, F., Lagares, D., Choi, K.M., Stopfer, L., Marinković, A., Vrbanac, V., Probst, C.K., Hiemer, S.E., Sisson, T.H., Horowitz, J.C., et al. (2015). Mechanosignaling through YAP and TAZ drives fibroblast activation and fibrosis. Am. J. Physiol. Lung Cell. Mol. Physiol. *308*, L344–L357.

Luedde, T., Kaplowitz, N., and Schwabe, R.F. (2014). Cell death and cell death responses in liver disease: mechanisms and clinical relevance. Gastroenterology *147*, 765–783.e4.

Machado, M.V., Michelotti, G.A., Pereira, T.A., Xie, G., Premont, R., Cortez-Pinto, H., and Diehl, A.M. (2015). Accumulation of duct cells with activated YAP parallels fibrosis progression in non-alcoholic fatty liver disease. J. Hepatol. *63*, 962–970.

Mederacke, I., Hsu, C.C., Troeger, J.S., Huebener, P., Mu, X., Dapito, D.H., Pradere, J.P., and Schwabe, R.F. (2013). Fate tracing reveals hepatic stellate cells as dominant contributors to liver fibrosis independent of its aetiology. Nat. Commun. *4*, 2823.

Mitani, A., Nagase, T., Fukuchi, K., Aburatani, H., Makita, R., and Kurihara, H. (2009). Transcriptional coactivator with PDZ-binding motif is essential for normal alveolarization in mice. Am. J. Respir. Crit. Care Med. *180*, 326–338.

Miura, K., Yang, L., van Rooijen, N., Brenner, D.A., Ohnishi, H., and Seki, E. (2013). Toll-like receptor 2 and palmitic acid cooperatively contribute to the development of nonalcoholic steatohepatitis through inflammasome activation in mice. Hepatology *57*, 577–589.

Mu, X., Español-Suñer, R., Mederacke, I., Affò, S., Manco, R., Sempoux, C., Lemaigre, F.P., Adili, A., Yuan, D., Weber, A., et al. (2015). Hepatocellular carcinoma originates from hepatocytes and not from the progenitor/biliary compartment. J. Clin. Invest. *125*, 3891–3903.

Nishio, M., Sugimachi, K., Goto, H., Wang, J., Morikawa, T., Miyachi, Y., Takano, Y., Hikasa, H., Itoh, T., Suzuki, S.O., et al. (2016). Dysregulated YAP1/TAZ and TGF-β signaling mediate hepatocarcinogenesis in Mob1a/1b-deficient mice. Proc. Natl. Acad. Sci. USA *113*, E71–E80.

Piersma, B., Bank, R.A., and Boersema, M. (2015). Signaling in Fibrosis: TGF-β, WNT, and YAP/TAZ Converge. Front Med (Lausanne) *2*, 59.

Puche, J.E., Saiman, Y., and Friedman, S.L. (2013). Hepatic stellate cells and liver fibrosis. Compr. Physiol. *3*, 1473–1492.

Rawson, R.B. (2006). An ARC light on lipid metabolism. Cell Metab. *4*, 181–183.

Razzaque, M.S., Soegiarto, D.W., Chang, D., Long, F., and Lanske, B. (2005). Conditional deletion of Indian hedgehog from collagen type 2alpha1-expressing cells results in abnormal endochondral bone formation. J. Pathol. *207*, 453–461.

Rinella, M.E. (2015). Nonalcoholic fatty liver disease: a systematic review. JAMA *313*, 2263–2273.

Saito, A., and Nagase, T. (2015). Hippo and TGF-β interplay in the lung field. Am. J. Physiol. Lung Cell. Mol. Physiol. *309*, L756–L767.

Shimamura, T., Fujisawa, T., Husain, S.R., Kioi, M., Nakajima, A., and Puri, R.K. (2008). Novel role of IL-13 in fibrosis induced by nonalcoholic steatohepatitis and its amelioration by IL-13R-directed cytotoxin in a rat model. J. Immunol. *181*, 4656–4665.

Singh, S., Allen, A.M., Wang, Z., Prokop, L.J., Murad, M.H., and Loomba, R. (2015). Fibrosis progression in nonalcoholic fatty liver vs nonalcoholic steatohepatitis: a systematic review and meta-analysis of paired-biopsy studies. Clin. Gastroenterol. Hepatol. *13*, 643–654.e1, 9, quiz e39–e40.

Subramanian, S., Goodspeed, L., Wang, S., Kim, J., Zeng, L., Ioannou, G.N., Haigh, W.G., Yeh, M.M., Kowdley, K.V., O'Brien, K.D., et al. (2011). Dietary cholesterol exacerbates hepatic steatosis and inflammation in obese LDL receptor-deficient mice. J. Lipid Res. *52*, 1626–1635.

Syn, W.K., Oo, Y.H., Pereira, T.A., Karaca, G.F., Jung, Y., Omenetti, A., Witek, R.P., Choi, S.S., Guy, C.D., Fearing, C.M., et al. (2010). Accumulation of natural killer T cells in progressive nonalcoholic fatty liver disease. Hepatology *51*, 1998–2007.

Syn, W.K., Choi, S.S., Liaskou, E., Karaca, G.F., Agboola, K.M., Oo, Y.H., Mi, Z., Pereira, T.A., Zdanowicz, M., Malladi, P., et al. (2011). Osteopontin is induced by hedgehog pathway activation and promotes fibrosis progression in nonalcoholic steatohepatitis. Hepatology *53*, 106–115.

Teratani, T., Tomita, K., Suzuki, T., Oshikawa, T., Yokoyama, H., Shimamura, K., Tominaga, S., Hiroi, S., Irie, R., Okada, Y., et al. (2012). A high-cholesterol diet exacerbates liver fibrosis in mice via accumulation of free cholesterol in hepatic stellate cells. Gastroenterology *142*, 152–164.e10.

Van Rooyen, D.M., Larter, C.Z., Haigh, W.G., Yeh, M.M., Ioannou, G., Kuver, R., Lee, S.P., Teoh, N.C., and Farrell, G.C. (2011). Hepatic free cholesterol accumulates in obese, diabetic mice and causes nonalcoholic steatohepatitis. Gastroenterology *141*, 1393–1403, 1403.e1–1403.e5.

White, D.L., Kanwal, F., and El-Serag, H.B. (2012). Association between nonalcoholic fatty liver disease and risk for hepatocellular cancer, based on systematic review. Clin. Gastroenterol. Hepatol. *10*, 1342–1359.e2, e2.

Wouters, K., van Gorp, P.J., Bieghs, V., Gijbels, M.J., Duimel, H., Lütjohann, D., Kerksiek, A., van Kruchten, R., Maeda, N., Staels, B., et al. (2008). Dietary cholesterol, rather than liver steatosis, leads to hepatic inflammation in hyperlipidemic mouse models of nonalcoholic steatohepatitis. Hepatology *48*, 474–486.

Xin, M., Kim, Y., Sutherland, L.B., Murakami, M., Qi, X., McAnally, J., Porrello, E.R., Mahmoud, A.I., Tan, W., Shelton, J.M., et al. (2013). Hippo pathway effector Yap promotes cardiac regeneration. Proc. Natl. Acad. Sci. USA *110*, 13839–13844.

Yamada, K., Mizukoshi, E., Sunagozaka, H., Arai, K., Yamashita, T., Takeshita, Y., Misu, H., Takamura, T., Kitamura, S., Zen, Y., et al. (2015). Characteristics of hepatic fatty acid compositions in patients with nonalcoholic steatohepatitis. Liver Int. *35*, 582–590.

Younossi, Z.M., Page, S., Rafiq, N., Birerdinc, A., Stepanova, M., Hossain, N., Afendy, A., Younoszai, Z., Goodman, Z., and Baranova, A. (2011). A biomarker panel for non-alcoholic steatohepatitis (NASH) and NASH-related fibrosis. Obes. Surg. *21*, 431–439.

Yu, F.X., Zhao, B., and Guan, K.L. (2015). Hippo pathway in organ size control, tissue homeostasis, and cancer. Cell *163*, 811–828.

Zanconato, F., Forcato, M., Battilana, G., Azzolin, L., Quaranta, E., Bodega, B., Rosato, A., Bicciato, S., Cordenonsi, M., and Piccolo, S. (2015). Genome-wide association between YAP/TAZ/TEAD and AP-1 at enhancers drives oncogenic growth. Nat. Cell Biol. *17*, 1218–1227.

Zanconato, F., Cordenonsi, M., and Piccolo, S. (2016). YAP/TAZ at the roots of cancer. Cancer Cell *29*, 783–803.

Zhao, B., Ye, X., Yu, J., Li, L., Li, W., Li, S., Yu, J., Lin, J.D., Wang, C.Y., Chinnaiyan, A.M., et al. (2008). TEAD mediates YAP-dependent gene induction and growth control. Genes Dev. *22*, 1962–1971.

Zhao, B., Li, L., Lei, Q., and Guan, K.L. (2010). The Hippo-YAP pathway in organ size control and tumorigenesis: an updated version. Genes Dev. *24*, 862–874.

Cell Metabolism, Volume *24*

Supplemental Information

Hepatocyte TAZ/WWTR1 Promotes Inflammation and Fibrosis in Nonalcoholic Steatohepatitis

Xiaobo Wang, Ze Zheng, Jorge Matias Caviglia, Kathleen E. Corey, Tina M. Herfel, Bishuang Cai, Ricard Masia, Raymond Chung, Jay H. Lefkowitch, Robert F. Schwabe, and Ira Tabas

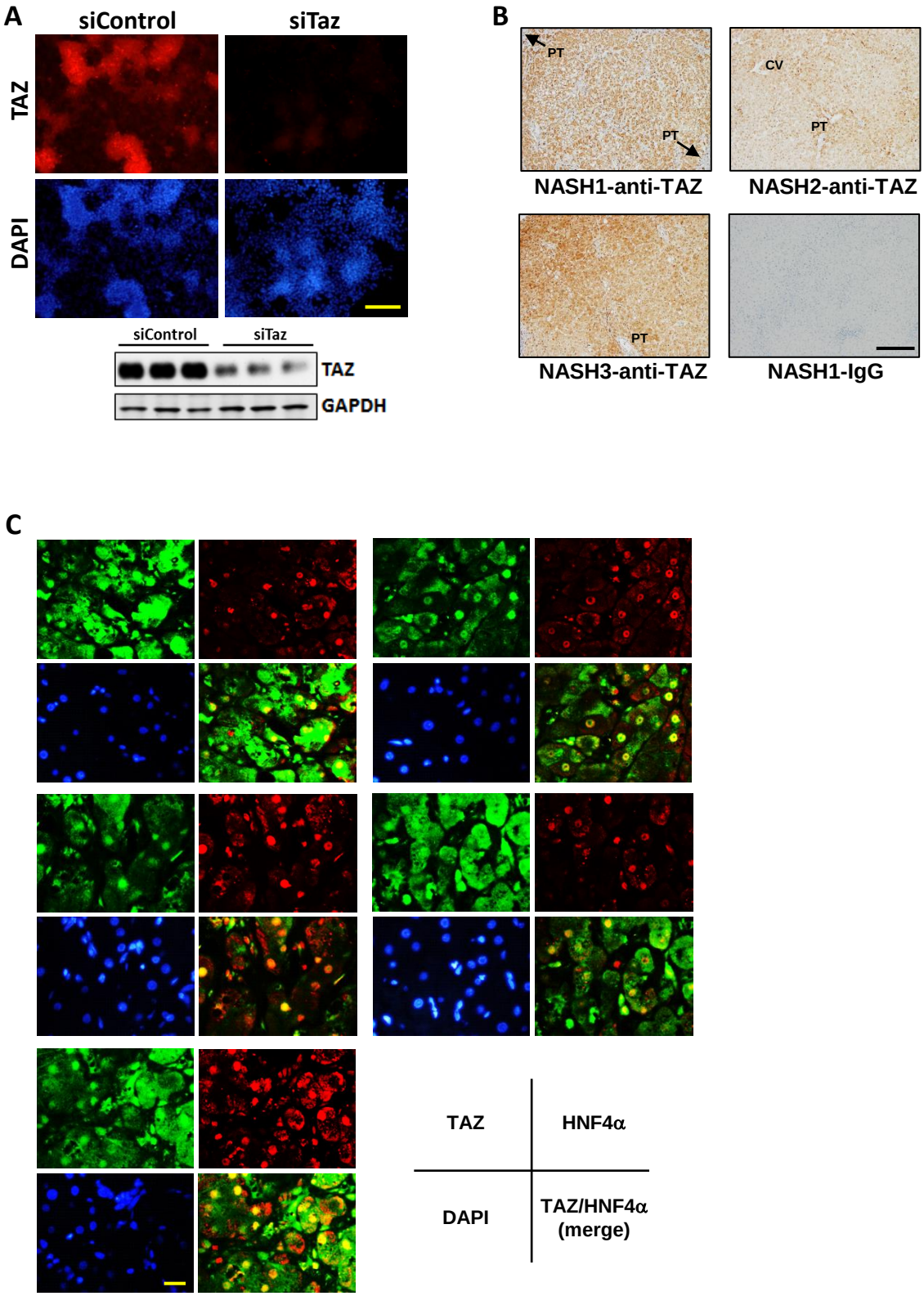
A
siControl
siTaz
TAZ
DAPI
siControl
siTaz
TAZ
GAPDH
B
PT
PT
NASH1-anti-TAZ
CV
PT
NASH2-anti-TAZ
PT
NASH3-anti-TAZ
NASH1-IgG
C
TAZ
HNF4α
DAPI
TAZ/HNF4α
(merge)

Figure S2

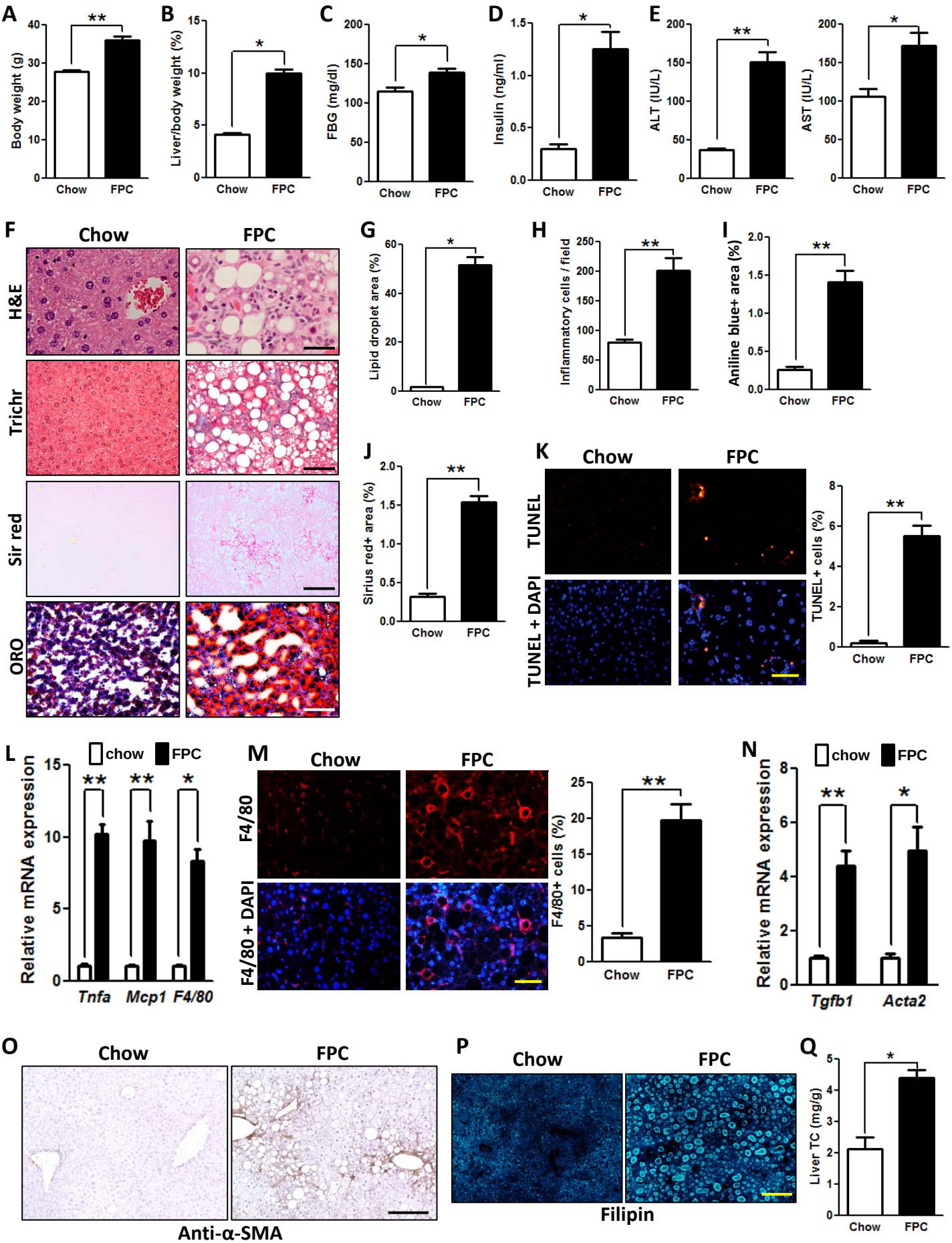
A
Body weight (g)
Chow
FPC
B
Liver/body weight (%)
C
FBG (mg/dl)
D
Insulin (ng/ml)
E
ALT (IU/L)
AST (IU/L)
F
Chow
FPC
H&E
Trichr
Sir red
ORO
G
Lipid droplet area (%)
H
Inflammatory cells / field
I
Aniline blue+ area (%)
J
Sirius red+ area (%)
K
TUNEL
TUNEL + DAPI
TUNEL+ cells (%)
L
chow
FPC
Relative mRNA expression
Tnfa
Mcp1
F4/80
M
F4/80
F4/80 + DAPI
F4/80+ cells (%)
N
Tgfb1
Acta2
O
Anti-α-SMA
P
Filipin
Q
Liver TC (mg/g)

Figure S3

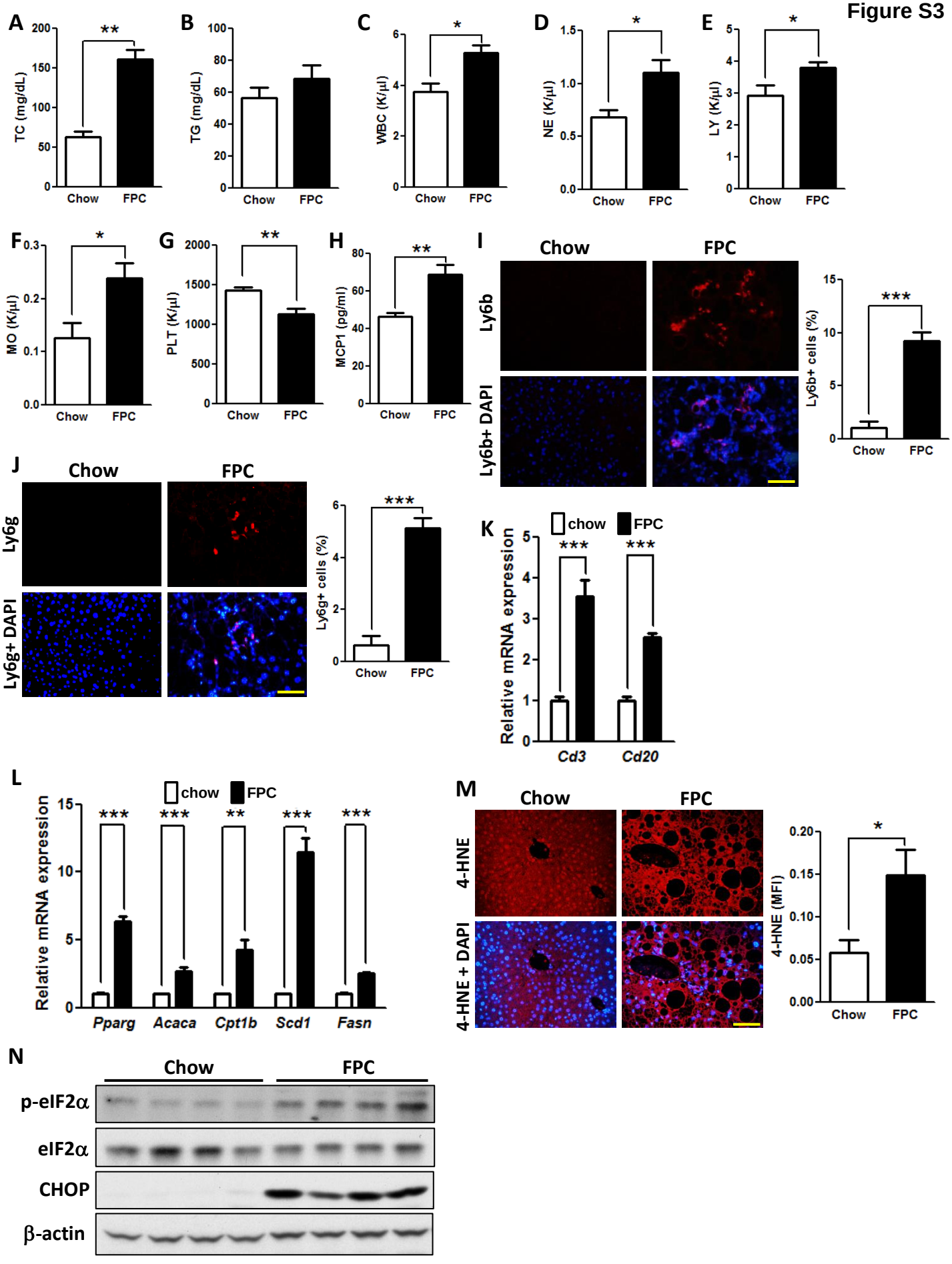
A
TC (mg/dL)
B
TG (mg/dL)
C
WBC (K/μl)
D
NE (K/μl)
E
LY (K/μl)
F
MO (K/μl)
G
PLT (K/μl)
H
MCP1 (pg/ml)
Chow
FPC
I
Ly6b
Ly6b+ DAPI
Ly6b+ cells (%)
J
Ly6g
Ly6g+ DAPI
Ly6g+ cells (%)
K
chow
FPC
Relative mRNA expression
Cd3
Cd20
L
Pparg
Acaca
Cpt1b
Scd1
Fasn
M
4-HNE
4-HNE + DAPI
4-HNE (MFI)
N
p-eIF2α
eIF2α
CHOP
β-actin

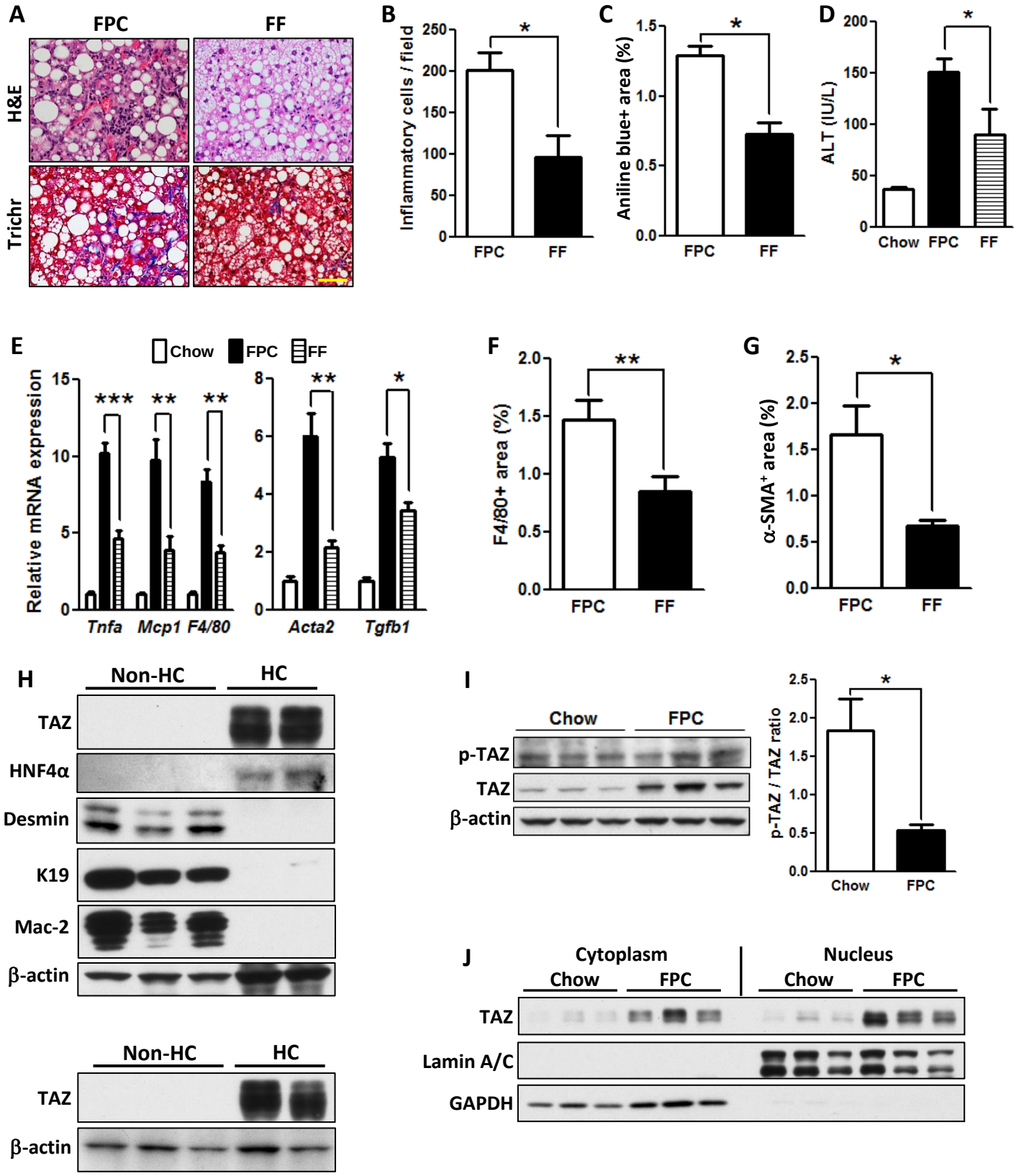
A
FPC
FF
H&E
Trichr
B
Inflammatory cells / field
FPC
FF
C
Aniline blue+ area (%)
FPC
FF
D
ALT (IU/L)
Chow
FPC
FF
E
Chow
FPC
FF
Relative mRNA expression
Tnfa
Mcp1
F4/80
Acta2
Tgfb1
F
F4/80+ area (%)
FPC
FF
G
α-SMA+ area (%)
FPC
FF
H
Non-HC
HC
TAZ
HNF4α
Desmin
K19
Mac-2
β-actin
Non-HC
HC
TAZ
β-actin
I
Chow
FPC
p-TAZ
TAZ
β-actin
p-TAZ / TAZ ratio
Chow
FPC
J
Cytoplasm
Nucleus
Chow
FPC
Chow
FPC
TAZ
Lamin A/C
GAPDH

Figure S5

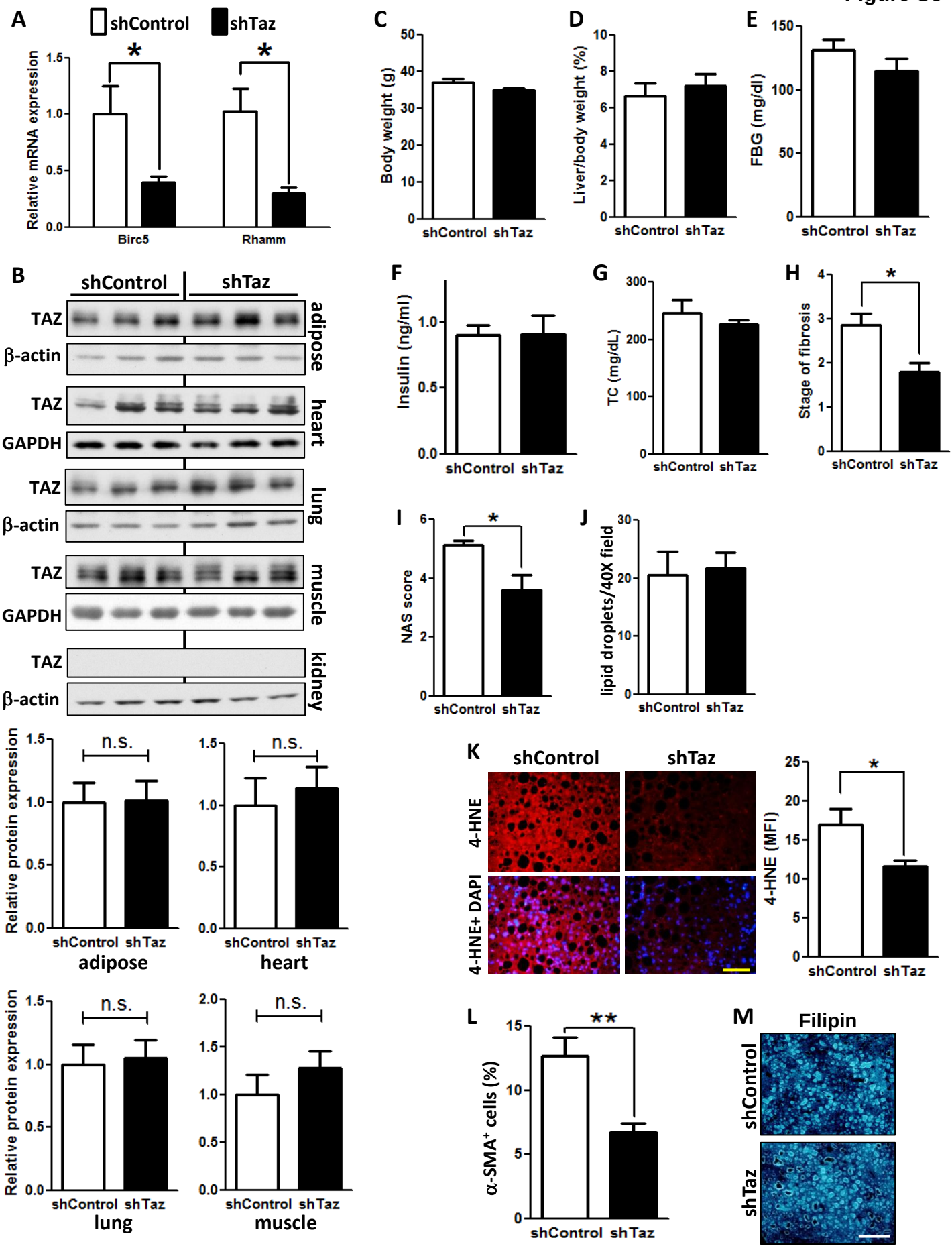
A
shControl
shTaz
Relative mRNA expression
Birc5
Rhamm
B
shControl
shTaz
TAZ
β-actin
adipose
TAZ
heart
GAPDH
TAZ
lung
β-actin
TAZ
muscle
GAPDH
TAZ
kidney
β-actin
C
Body weight (g)
shControl shTaz
D
Liver/body weight (%)
shControl shTaz
E
FBG (mg/dl)
shControl shTaz
F
Insulin (ng/ml)
shControl shTaz
G
TC (mg/dL)
shControl shTaz
H
Stage of fibrosis
shControl shTaz
I
NAS score
shControl shTaz
J
lipid droplets/40X field
shControl shTaz
Relative protein expression
n.s.
shControl shTaz
adipose
heart
lung
muscle
K
shControl
shTaz
4-HNE
4-HNE+ DAPI
4-HNE (MFI)
shControl shTaz
L
α-SMA+ cells (%)
shControl shTaz
M
Filipin
shControl
shTaz

Figure S6

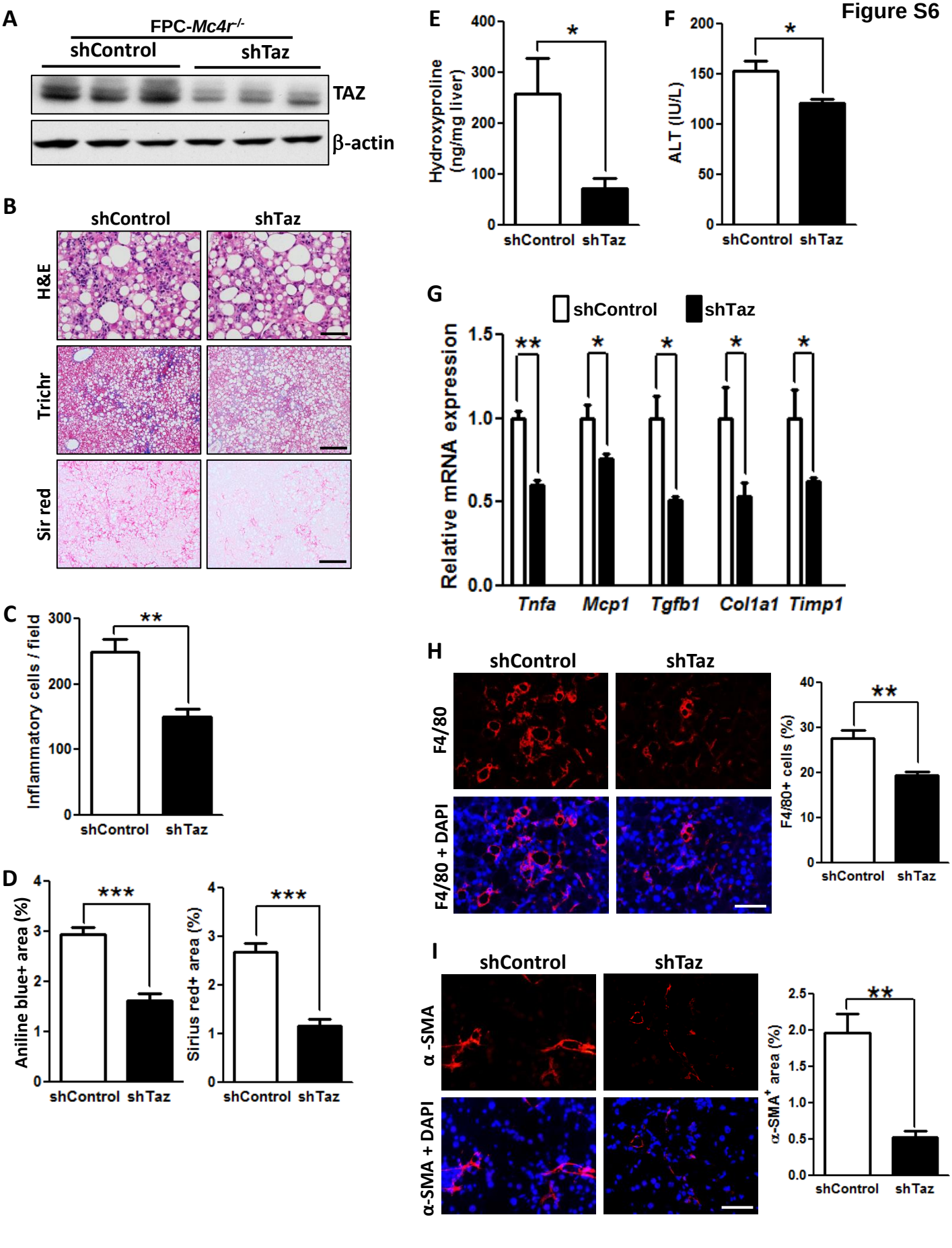
A
FPC-Mc4r-/-
shControl
shTaz
TAZ
β-actin
B
shControl
shTaz
H&E
Trichr
Sir red
C
Inflammatory cells / field
300
200
100
0
**
shControl
shTaz
D
Aniline blue+ area (%)
***
Sirius red+ area (%)
***
shControl
shTaz
E
Hydroxyproline (ng/mg liver)
400
300
200
100
0
*
shControl
shTaz
F
ALT (IU/L)
200
150
100
50
0
*
shControl
shTaz
G
shControl
shTaz
Relative mRNA expression
1.5
1.0
0.5
0.0
**
*
*
*
*
Tnfa
Mcp1
Tgfb1
Col1a1
Timp1
H
shControl
shTaz
F4/80
F4/80 + DAPI
F4/80+ cells (%)
40
30
20
10
0
**
shControl
shTaz
I
shControl
shTaz
α -SMA
α-SMA + DAPI
α-SMA+ area (%)
2.5
2.0
1.5
1.0
0.5
0.0
**
shControl
shTaz

Figure S7

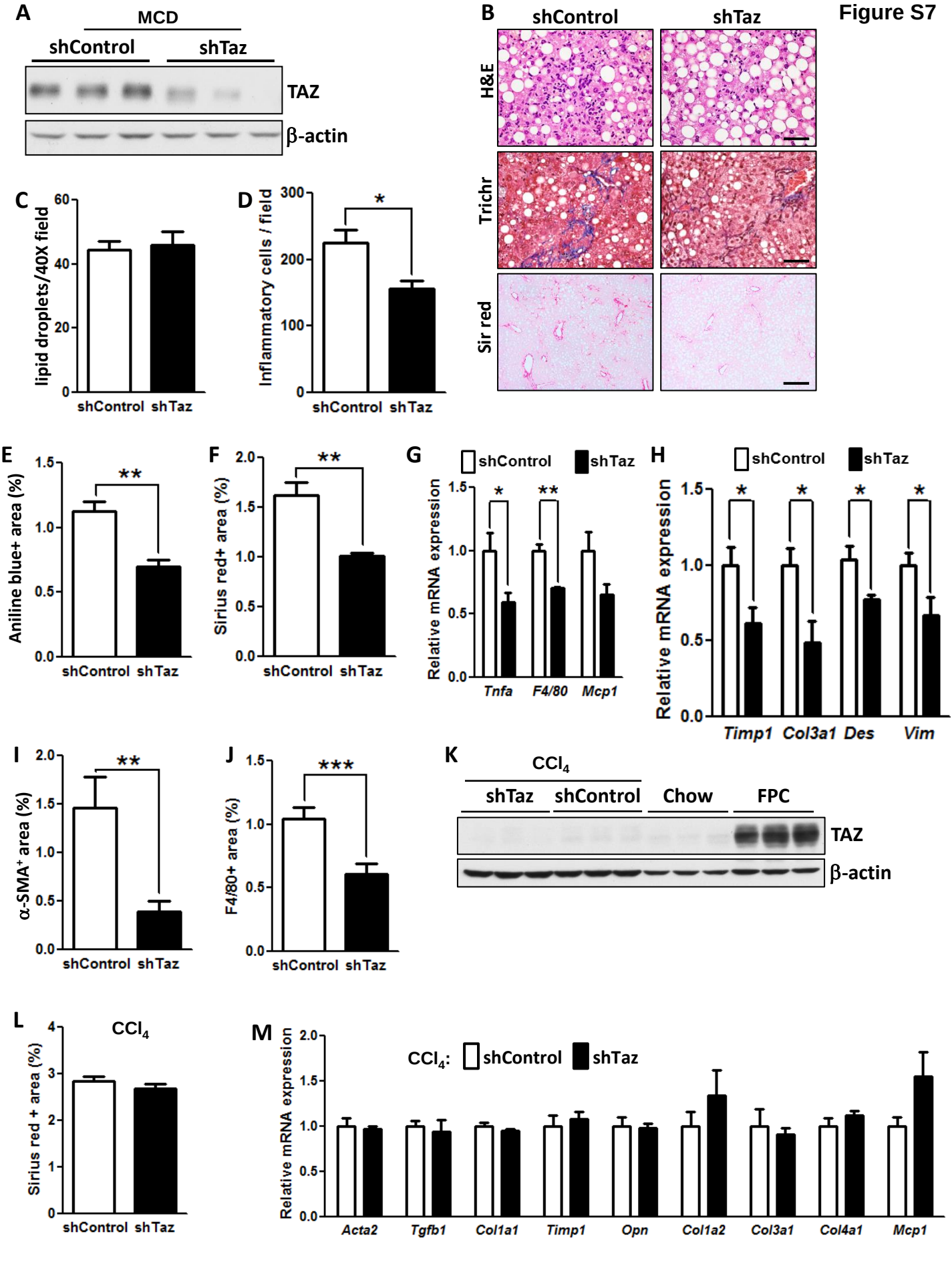
A
MCD
shControl
shTaz
TAZ
β-actin
B
shControl
shTaz
H&E
Trichr
Sir red
C
lipid droplets/40X field
shControl shTaz
D
Inflammatory cells / field
shControl shTaz
E
Aniline blue+ area (%)
shControl shTaz
F
Sirius red+ area (%)
shControl shTaz
G
shControl
shTaz
Relative mRNA expression
Tnfa
F4/80
Mcp1
H
shControl
shTaz
Relative mRNA expression
Timp1
Col3a1
Des
Vim
I
α-SMA+ area (%)
shControl shTaz
J
F4/80+ area (%)
shControl shTaz
K
CCl4
shTaz
shControl
Chow
FPC
TAZ
β-actin
L
CCl4
Sirius red + area (%)
shControl shTaz
M
CCl4:
shControl
shTaz
Relative mRNA expression
Acta2
Tgfb1
Col1a1
Timp1
Opn
Col1a2
Col3a1
Col4a1
Mcp1

Figure S8

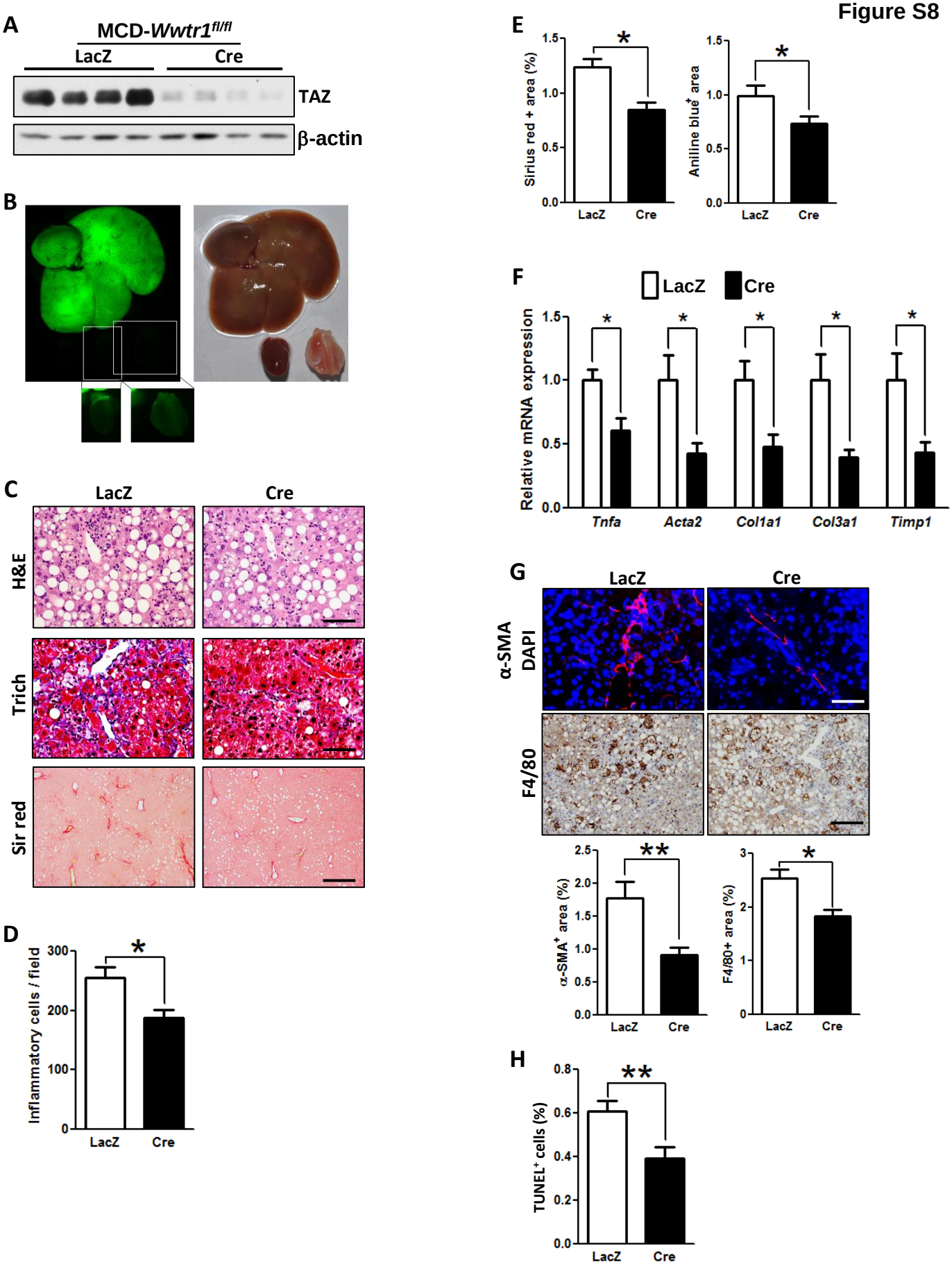
A
MCD-Wwtr1fl/fl
LacZ
Cre
TAZ
β-actin
B
C
LacZ
Cre
H&E
Trich
Sir red
D
Inflammatory cells / field
LacZ
Cre
E
Sirius red + area (%)
Aniline blue+ area
F
LacZ
Cre
Relative mRNA expression
Tnfa
Acta2
Col1a1
Col3a1
Timp1
G
α-SMA
DAPI
F4/80
α-SMA+ area (%)
F4/80+ area (%)
H
TUNEL+ cells (%)

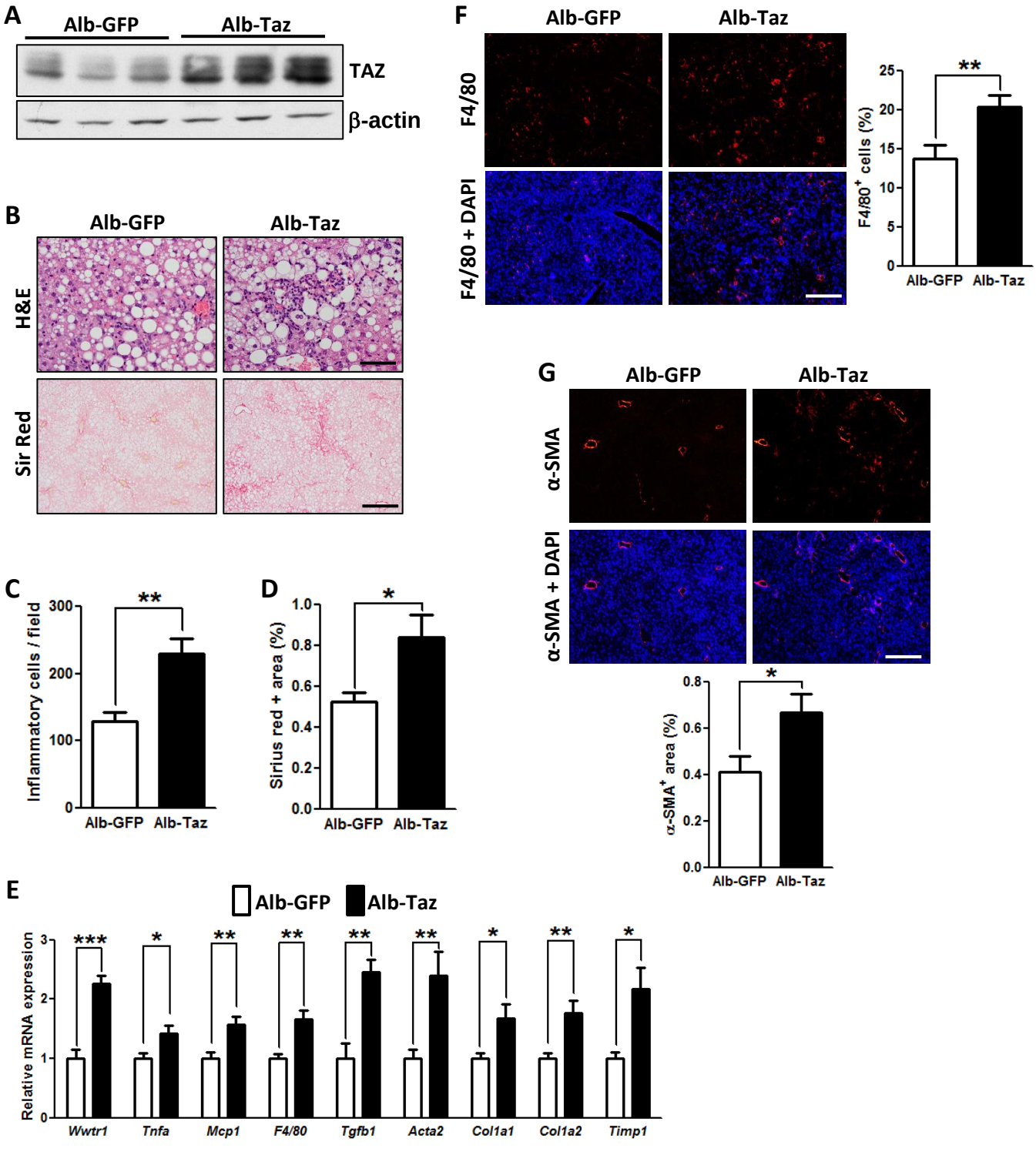
A
Alb-GFP
Alb-Taz
TAZ
β-actin
B
Alb-GFP
Alb-Taz
H&E
Sir Red
C
Inflammatory cells / field
300
200
100
0
**
Alb-GFP
Alb-Taz
D
Sirius red + area (%)
1.0
0.8
0.6
0.4
0.2
0.0
*
Alb-GFP
Alb-Taz
E
Alb-GFP
Alb-Taz
Relative mRNA expression
3
2
1
0
***
*
**
**
**
**
*
**
*
Wwtr1
Tnfa
Mcp1
F4/80
Tgfb1
Acta2
Col1a1
Col1a2
Timp1
F
Alb-GFP
Alb-Taz
F4/80
F4/80 + DAPI
F4/80+ cells (%)
25
20
15
10
5
0
**
Alb-GFP
Alb-Taz
G
Alb-GFP
Alb-Taz
α-SMA
α-SMA + DAPI
α-SMA+ area (%)
0.8
0.6
0.4
0.2
0.0
*
Alb-GFP
Alb-Taz

Supplemental Figure Legends

Figure S1 (Related to Figure 1). TAZ Expression in the Livers of Humans with NASH.

(A) As evidence that the anti-TAZ antibody used in the human liver immunofluorescence experiment in Figure 1A is specific, TAZ silencing in human HepG2 liver cells eliminates the anti-TAZ immunofluorescence signal (red) in these cells; DAPI stain for nuclei is shown in bottom panels. siControl, control RNA; siTaz, siRNA targeting Taz (*Wwtr1*); Bar, 100 µM. Efficiency of TAZ silencing is demonstrated by the HepG2 immunoblot.

(B) Sections of liver from 3 separate NASH subjects were immunostained for TAZ. PT, portal tract; CV, central vein. A section of liver from subject 1 was stained using control IgG. Bar, 500 µm.

(C) TAZ (green) and HNF4α (red nuclei) immunostaining in the livers of 5 separate human NASH specimens; for each image set, upper left = TAZ, upper right = HNF4α, lower left = DAPI (nuclei), and lower right = TAZ/HNF4α merge; Bar, 50µm.

Figure S2 (Related to Figure 1). FPC-fed Mice Develop Weight Gain, Insulin Resistance, and Features of NASH

The following parameters were measured in male C57BL/6J mice after 16 weeks on chow or FPC diet (*$p < 0.02$, **$p<0.0001$; mean ± SEM; n=6 mice/group):

(A-B) Body weight and liver:body weight ratio.

(C-E) Plasma fasting glucose, insulin, ALT, and AST.

(F) Staining of liver sections with H&E (1st row; Bar, 100µm), Masson's trichrome (Trichr) (2nd row; Bar, 100µm), Sirius red (Sir red) (3rd row; Bar, 500µm), and Oil Red O (ORO)/H&E (4th row; Bar, 100µm).

(G-J) Lipid droplet area, liver inflammatory cell number, and aniline blue- and Sirius red-positive area.

(K) TUNEL staining (red) and quantification; DAPI counterstain for nuclei is shown in bottom panels; Bar, 100 µm.

(L) mRNA levels of Tnfa, Mcp1, and F4/80 (Adgre1).

(M) F4/80 immunofluorescence (red) and quantification; merge with DAPI counterstain for nuclei (blue) is shown in bottom panels; Bar, 100 µm.

(N) mRNA levels of Tgfb1 and Acta2 (α-SMA).

(O) α-SMA immunohistochemistry; Bar, 200µm.

(P) Filipin staining; Bar, 200μm.
(Q) Liver cholesterol content.

Figure S3 (related to Figure 1). Effects of FPC Diet on Additional Metabolic Profile and Liver Parameters

The following parameters were measured in male C57BL/6J mice after 16 weeks on chow or FPC diet (*p < 0.05, **p < 0.01, ***p < 0.0001; mean ± SEM; n=6 mice/group):
(A-B) Plasma total cholesterol (TC) and triglyceride (TG).
(C-G) Total blood white blood cell (WBC), neutrophil (NE), lymphocyte (LY), monocyte (MO), and platelet (PLT) counts.
(H) Plasma MCP1.
(I) Ly6b immunofluorescence staining (red) of liver and quantification; DAPI counterstain for nuclei is shown in bottom panels; Bar, 100μm.
(J) Ly6g immunofluorescence (red) of liver and quantification; DAPI counterstain for nuclei is shown in bottom panels; Bar, 100μm.
(K) Cd3 (pan-T lymphocyte marker) and Cd20 (pan-B lymphocyte marker) mRNA.
(L) mRNAs of the indicated lipid metabolic enzymes.
(M) 4-hydroxynonenal (4-HNE) immunofluorescence (red) and quantification; DAPI counterstain for nuclei is shown in bottom panels; Bar, 100μm.
(N) Immunoblots of liver phospho- and total eIF2α and CHOP, with β-actin as loading control.

Figure S4 (Related to Figure 1). Comparison of Liver Parameters in Mice Fed the FPC *vs*. FF Diet for 16 Weeks and Analyses of TAZ Expression in FPC-Fed Mice.

The following parameters were measured in male C57BL/6J mice after 16 weeks on chow, FPC, or FF diet (*p < 0.05, **p < 0.01, ***p < 0.0001; mean ± SEM; n=5 mice/group):
(A) Staining of liver sections for H&E (upper panels) and Masson's trichrome (Trichr) (lower panels); Bar, 100 μm.
(B-C) Hepatic inflammatory cells and aniline blue-positive area.
(D) Plasma ALT.
(E) mRNA levels of Tnfa, Mcp1, F4/80 (Adgre1), Acta2 (α-SMA), and Tgfb1.
(F) Quantification of percent F4/80^{+} area as assessed by immunofluorescence microscopy.

(G) Quantification of percent α-SMA$^+$ area as assessed by immunofluorescence microscopy.
(H) Immunoblot of TAZ in hepatocytes and non-hepatocyte cells isolated from the livers of mice fed the FPC diet for 10 weeks. The lower image shows the TAZ blot under equal loading condition. The following markers were used: HNF4α, hepatocytes; desmin, HSCs; K19, ductal cells; Mac-2, Kupffer cells. β-actin was used as the loading control.
(I) Immunoblot of phospho-TAZ and total TAZ of liver extracts from 16-week chow-fed and FPC-fed mice; β-actin served as the loading control. The graph shows the densitometric ratios of phospho-TAZ:total TAZ (*$p < 0.04$; mean ± SEM; n=3).
(J) Immunoblot of TAZ in cytoplasmic and nuclear fractions of livers from 16-week chow-fed and FPC-fed mice. Lamin A/C and GAPDH were used as markers and loading controls for nucleus and cytoplasm, respectively.

Figure S5 (Related to Figure 2). Effects of TAZ Silencing on Metabolic Profile and Additional Liver Parameters in 16-Week FPC-Fed Mice

The following parameters were measured in male C57BL/6J mice treated with AAV8-H1-shTaz or control vector and then fed the FPC diet for 16 weeks (*$p < 0.01$, **$p < 0.001$; mean ± SEM; n=10 mice/group):
(A) mRNA levels of Birc5 and Rhamm.
(B) The indicated tissues, where "muscle" refers to gastrocnemius muscle and "adipose" to epididymal fat, were immunoblotted for TAZ and loading controls and quantified by densitometric ratio analysis (n=3 mice; n.s., non-significant).
(C-D) Body weight and liver:body weight ratio.
(E-G) Fasting blood glucose, plasma insulin, and total plasma cholesterol (TC).
(H-I) Stage of fibrosis and NAS score.
(J) Hepatic lipid droplet number.
(K) 4-hydroxynonenal (4-HNE) immunofluorescence (red) and quantification; DAPI counterstain for nuclei is shown in bottom panels; Bar, 100 μm.
(L) α-SMA$^+$ cells.
(M) Filipin staining; Bar, 500 μm.

Figure S6 (Related to Figure 2). TAZ Silencing Reduces Liver Inflammation and Fibrosis in FPC-Fed *Mc4r*$^{-/-}$ Hyperphagic Mice

The following parameters were measured in male Mc4r-/- mice treated with AAV8-H1-shTaz or control vector and then fed the FPC diet for 16 weeks (*p < 0.05, **p < 0.01, ***p < 0.0001, mean ± SEM; n=5 mice/group):
(A) Immunoblot of TAZ, with β-actin as loading control.
(B) Staining of liver sections for H&E (upper panels; Bar, 100 μm), Masson's trichrome (Trichr) (middle panels; Bar, 500 μm), and Sirius red (Sir red) (lower panels; Bar, 500 μm).
(C) Hepatic inflammatory cells.
(D) Aniline blue- and Sirius red-positive area.
(E) Hydroxyproline content.
(F) Plasma ALT.
(G) mRNA levels of Tnfa, Mcp1, Tgfb1, Col1a1, and Timp1.
(H) F4/80 immunofluorescence (red) and quantification; DAPI counterstain for nuclei is shown in bottom panels; Bar, 100 μm.
(I) α-SMA immunofluorescence (red) and quantification; DAPI counterstain for nuclei is shown in bottom panels; Bar, 100 μm.

Figure S7 (related to Figure 2). Taz Silencing in MCD-Fed Mice Reduces Liver Inflammation and Fibrosis

(A-J) The following parameters were measured in male mice treated with AAV8-H1-shTaz or control vector and then fed the MCD diet for 8 weeks (*p < 0.05, **p < 0.01, ***p < 0.0001; mean ± SEM; n=5 mice/group):
(A) Immunoblot of TAZ, with β-actin as loading control.
(B) Staining of liver sections for H&E (upper panels; Bar, 100μm), Masson's trichrome (Trichr) (middle panels; Bar, 100μm), and Sirius red (Sir red) (lower panels; Bar, 500μm).
(C-D) Hepatic lipid droplet and inflammatory cell numbers.
(E-F) Aniline blue- and Sirius red-positive area.
(G) mRNA levels of Tnfa, F4/80 (Adgre1), and Mcp1.
(H) mRNA levels of Timp1, Col3a1, Des, and Vim.
(I) α-SMA$^+$ area.
(J) F4/80$^+$ area.
(K-M) The following parameters were measured in male mice treated with for AAV8-H1-shTaz or control vector and then administered with CCl4 for 6 weeks.
(K) Immunoblot of TAZ, with β-actin as loading control.

(L) Sirius red positive area.
(M) mRNA levels of the indicated genes related to fibrosis.

Figure S8 (Related to Figure 2). AAV8-TBG-Cre-Mediated Hepatocyte Taz Deletion in MCD-fed *Wwtr1*$^{fl/fl}$ Mice Reduces Liver Inflammation and Fibrosis

The following parameters were measured in male *Wwtr1*$^{fl/fl}$ mice treated with AAV8-TBG-Cre or AAV8-TBG-LacZ and then fed the MCD diet for 8 weeks (*p < 0.05, **p < 0.01, ***p < 0.0001; mean ± SEM; n=5 mice/group):
(A) Immunoblot of TAZ, with β-actin as loading control.
(B) Fluorescent images and photographs of liver, heart (bottom center), and gastrocnemius muscle (bottom right) in ZsGreen flox-reporter mice treated with AAV8-TBG-Cre. The 2 images below the fluorescence image show the heart and gastrocnemius muscle at a 10-fold higher gain setting.
(C) Staining of liver sections for H&E (upper panels; Bar, 100μm), Sirius red (Sir red) (middle panels; Bar, 500μm) and Masson's trichrome (Trichr) (lower panels; Bar, 500μm).
(D) Inflammatory cell numbers.
(E) Aniline blue- and Sirius red-positive area.
(F) mRNA levels of Tnfa, Acta2, Col1a1, Col3a1 and Timp1.
(G) α-SMA immunofluorescence (red) (upper panels; DAPI counterstain for nuclei; Bar, 200 μm) and F4/80 immunohistochemistry (lower panels; Bar, 200 μm).
(H) TUNEL^{+} cells.

Figure S9 (Related to Figure 4). Genetically mediated TAZ Expression in Hepatocytes Promotes Liver Inflammation and Fibrosis in a Mouse Model of Steatosis

The following parameters were measured in male C57BL/6J mice fed the FF diet for 16 weeks, with AAV8-Alb-Taz or Alb-GFP vector administered at the 8-week time point (*p < 0.05, **p < 0.01, ***p < 0.0001, mean ± SEM; n=5 mice/group):
(A) Immunoblot of TAZ, with β-actin as loading control.
(B) Staining of liver sections for H&E (upper panels; Bar, 100 μm) and Sirius red (Sir red) (lower panels; Bar, 500 μm).
(C) Hepatic inflammatory cells.
(D) Sirius red-positive area.
(E) mRNA levels of Wwtr1, Tnfa, Mcp1, F4/80, Tgfb1, Acta2, Col1a1, Col1a2 and Timp1.

(F) F4/80 immunofluorescence (red) and quantification; DAPI counterstain for nuclei is shown in bottom panels; Bar, 500 μm.
(G) α-SMA immunofluorescence (red) and quantification; DAPI counterstain for nuclei is shown in bottom panels; Bar, 500 μm.

Supplemental Tables

Table S1 (Related to Figure 1). Composition of the FPC diet.

Food Component	**g/kg diet**
Casein, "Vitamin-Free"	140.0
Sucrose	341.5
Maltodextrin	119.6
Vegetable shortening, hydrogenated (Primex)	190.0
Anhydrous milk fat	60.0
Palmitic acid (Nu-Chek-Prep N-16A or Sigma W283207)	40.0
Cholesterol	12.5
Cellulose	50.0
Mineral mix, AIN-76 (170915)	35.0
Calcium carbonate	4.0
Vitamin mix, w/o choline, A, D, E (83171)	5.0
Vitamin E, DL-alpha tocopheryl acetate	0.1
Vitamin A palmitate	0.04
Vitamin D3, cholecalciferol	0.0044
Choline dihydrogen citrate	2.28
Drinking water	**g/L**
55% glucose/45% fructose solution (w/w)	42

Table S2 (Related to Figure 1). Caloric composition of chow, fructose-palmitate-cholesterol (FPC), and "fast food" (FF) diets. Estimated nutrient data were calculated from published values and direct analytical testing of raw materials.

	Chow diet	FPC diet	FF diet
Diet source and #	LabDiet Rodent Diet 20, #5053	Teklad Diets TD.140154	TestDiet #1810060
Macronutrients			
Protein, % by weight	21.0	12.6	17.4
Carbohydrate, % by weight	53.5	46.2	49.9
Fat, % by weight	5.0	28.8	20.0
Protein, % kcal	24.5	10.2	15.5
Carbohydrate, % kcal	62.4	37.4	44.4
Fat, % kcal	13.1	52.4	40.1
Methionine, g/kg	6.2	3.4	8.0
Sucrose, % by weight	3.2	34	34
Cholesterol, % by weight	0.01	1.25	0.2
Vitamin E, IU/kg	99	50	50
Choline, mg/kg	1490	915	918
SFA, % total fatty acids	20.7	46	70
cis-MUFA, % total fatty acids	26	24	26.7
cis-PUFA, % total fatty acids	53.3	4	3.3
Trans-fats, % total fatty acids	N/A	26	0
Trans-fats, % by weight	N/A	7	0
Palmitic Acid, % by weight	N/A	8.7	5.2

Table S3 (Related to Figure 1). Saponified fatty acid content of the livers of mice fed the FPC diet for 16 wks (µmol/g liver). P values were calculated using one-way ANOVA with post-hoc Tukey test.

FA	Chow			FPC			P value
	Average	SD	% of total FA	Average	SD	% of total FA	
C14:1	1.581	0.3316	0.1092	3.351	0.2631	0.0964	0.0054
C14	12.369	2.3932	0.8544	27.687	1.0312	0.7962	0.0025
C16:1	81.675	15.447	5.6421	351.48	24.869	10.107	0.0009
C16	233.65	29.845	16.14	420.04	9.6215	12.079	0.0018
C18:3	43.305	6.1274	2.9915	10.509	0.2135	0.3022	0.0025
C18:2	513.51	70.787	35.473	159.21	6.8258	4.5782	0.0031
C18:1	383.23	51.698	26.473	2347.5	77.063	67.506	3E-05
C18	49.641	11.68	3.4292	44.349	4.7849	1.2753	0.5944
C20:5	13.23	2.0541	0.9139	0.63	0.2154	0.0181	0.0021
C20:4	47.481	5.6404	3.28	34.143	3.9159	0.9818	0.0243
C20:1	4.317	0.8123	0.2982	63.795	6.0916	1.8345	0.0006
C20	0.582	0.1372	0.0402	1.386	0.2549	0.0399	0.0105
C22:6	62.589	8.0908	4.3236	10.032	1.2551	0.2885	0.0011
C22:1	0	0	0	3.051	0.7256	0.0877	0.0053
C22	0.423	0.1254	0.0292	0.36	0.0945	0.0104	0.4897
C24:1	0		0	0		0	
C24	0		0	0		0	

Table S4, (Related to Figures 1, 2, 3, 4, 5, 6, ,7). Primers used for QPCR.

Primers	Sequences
Hprt F	TCAGTCAACGGGGGACATAAA
Hprt R	GGGGCTGTACTGCTTAACCAG
Taz (*Wwtr1*) F	CATGGCGGAAAAAGATCCTCC
Taz (*Wwtr1*) R	GTCGGTCACGTCATAGGACTG
Tgfb1 F	CTCCCGTGGCTTCTAGTGC
Tgfb1 R	GCCTTAGTTTGGACAGGATCTG
Acta2 F	ATGCTCCCAGGGCTGTTTTCCCAT
Acta2 R	GTGGTGCCAGATCTTTTCCATGTCG
Vim F	TTTCTCTGCCTCTGCCAAC
Vim R	TCTCATTGATCACCTGTCCATC
Des F	CTAAAGGATGAGATGGCCCG
Des R	GAAGGTCTGGATAGGAAGGTTG
Col1a1 F	GCTCCTCTTAGGGGCCACT
Col1a1 R	CCACGTCTCACCATTGGGG
Col1a2 F	GTAACTTCGTGCCTAGCAACA
Col1a2 R	CCTTTGTCAGAATACTGAGCAGC
Col3a1 F	CTGTAACATGGAAACTGGGGAAA
Col3a1 R	CCATAGCTGAACTGAAAACCACC
Col4a1 F	CTGGCACAAAAGGGACGAG
Col4a1 R	ACGTGGCCGAGAATTTCACC
F4/80 (*Adgre1*) F	ACCACAATACCTACATGCACC
F4/80 (*Adgre1*) R	AAGCAGGCGAGGAAAAGATAG
Tnfa F	CTTCTGTCTACTGAACTTCGGG
Tnfa R	CAGGCTTGTCACTCGAATTTTG
Mcp1 F	TTAAAAACCTGGATCGGAACCAA
Mcp1 R	GCATTAGCTTCAGATTTACGGGT
Ihh F	CTCTTGCCTACAAGCAGTTCA
Ihh R	CCGTGTTCTCCTCGTCCTT
Gli2 F	CAACGCCTACTCTCCCAGAC
Gli2 R	GAGCCTTGATGTACTGTACCAC
Gli3 F	CACAGCTCTACGGCGACTG
Gli3 R	CTGCATAGTGATTGCGTTTCTTC
Opn F	CTGACCCATCTCAGAAGCAGAATCT
Opn R	TCCATGTGGTCATGGCTTTCATTGG
Timp1 F	CTCAAAGACCTATAGTGCTGGC
Timp1 R	CAAAGTGACGGCTCTGGTAG
Cpt1b F	GCACACCAGGCAGTAGCTTT
Cpt1b R	CAGGAGTTGATTCCAGACAGGTA
Pparg F	TCGCTGATGCACTGCCTATG
Pparg R	GAGAGGTCCACAGAGCTGATT
Scd1 F	CTGACCTGAAAGCCGAGAAG
Scd1 R	AGAAGGTGCTAACGAACAGG
Fasn F	AAGTCCCAGAAATCGCCTATG

Fasn R	GGTATGGTTTCACGACTGGAG
Acaca F	ATGGGCGGAATGGTCTCTTTC
Acaca R	TGGGGACCTTGTCTTCATCAT
Cd3 F	ATGCGGTGGAACACTTTCTGG
Cd3 R	GCACGTCAACTCTACACTGGT
Cd20 F	AACCTGCTCCAAAAGTGAACC
Cd20 R	CCCAGGGTAATATGGAAGAGGC
Ihh intron 1F	CAATCATTGACAGCGAGGGC
Ihh intron 1F	GGTGTAGCTCGGTTCTGGTAG
Ihh non-specific F	GGTGTAGCTCGGTTCTGGTAG
Ihh non-specific R	TCACCTGGGACTCCATTTGC

Hprt, hypoxanthine guanine phosphoribosyl transferase; *Taz* (*Wwtr*1), WW domain containing transcription regulator 1; *Tgfb1*, transforming growth factor, beta 1; *Acta2*, a-smooth muscle actin; *Vim*, vimentin; *Des*, desmin; *Col1a1*, collagen type I alpha 1; *Col1a2*, collagen type I alpha 2; *Col3a1*, collagen, type III, alpha 1; *Col4a1*, collagen, type IV, alpha 1; *F4/80* (*Adgre1*), adhesion G protein-coupled receptor E1; *Tnfa*, tumor necrosis factor-a ; *Mcp1*, monocyte chemoattractant protein-1; *Ihh*, Indian hedgehog; *Gli2*, *GLI* family zinc finger 2;*Gli3*, *GLI* family zinc finger 3; *Opn*, osteopontin; *Timp1*, tissue inhibitor of metalloproteinase 1; *Cpt1b*, carnitine palmitoyltransferase 1B; *Pparg*, peroxisome proliferator-activated receptor-γ; *Scd1*, stearoyl-CoA desaturase; *Fasn*, fatty acid synthase; *Acaca*, acetyl-CoA carboxylase-a; *Cd3*, *CD3* antigen; *Cd20*, B-lymphocyte antigen; *Ihh* intron: specific TAZ/TEAD binding area in 1st intron of *Ihh* gene; *Ihh* non-specific: non-specific TAZ/TEAD binding site in mouse *Ihh* gene distal promoter.

Supplemental Experimental Procedures

Reagents and Antibodies

The following antibodies were used for immunoblots: GAPDH (#3683), β-actin (#5125), CHOP (#5554), TAZ (#8418), p-eIF2α (#3398), eIF2α (#5324), Lamin A/C (#4777) from Cell Signaling; p-TAZ (sc-17610) and Col1a1 (sc-8784) from Santa Cruz; Ihh (ab39634) from Abcam; Mac-2 (CL8942AP) from Accurate Chem; Desmin (RB-9014-P) from ThermoFisher; K19 (TROMA-III) from DSHB; and Timp1 (AF980) from R & D. The following antibodies were using for immunostaining of liver: α-SMA (ACTA2) (C6198, F3777), TAZ (HPA007415) from Sigma; F4/80 (MCA497GA) from AbD Serotec; Ly6g (#127601) from Biolegend; Ly6b (MCA771G) from Bio-Rad; OPN (AF808) from R & D; 4-hydroxynonenal (4-HNE) (AB5605) from Millipore; and HNF4α (sc-6556) from Santa Cruz. The following plasma assay kits were used in this study: insulin ELISA (#90080) from Crystal Chem; MCP1 ELISA (#88-7391-22) from eBiosciences; cholesterol (#439-17501) and triglyceride (#465-09791, #461-09891) from Wako; and ALT (#006A-CR) and AST (#004A-CR) from BQ Kits, Inc. Adeno-associated virus subtype 8 (AAV8)-shRNA targeting murine Taz was made by annealing complementary oligonucleotides (5'-CACCAcagccgaatctcgcaatgaatCTCGAGATTCATTGCGAG ATTCGGCTG-3'), which were then ligated into the self-complementary (sc) AAV8-RSV-GFP-H1 vector as described previously (Lisowski et al., 2014). AAV8-H1-shRNA targeting murine Ihh was made by annealing complementary oligonucleotides (5'-CACCAaccaccttcagtgatgtgcttaTCAAGAGTAAGCACATCA CTGAAGGTGGG-3'), which were then ligated into the scAAV-RSV-GFP-H1 vector as above. The resultant constructs were amplified by the Salk Institute Gene Transfer, Targeting, and Therapeutics Core. A fragment of intron 1of the murine Ihh gene, which includes a consensus TAZ/TEAD-binding sequence (AGGAATGC) and 500 bp upstream and downstream of this sequence, was cloned into a luciferase reporter plasmid (Addgene #64784) (Chang et al., 2007). A similar fragment, but containing a mutated TAZ/TEAD-binding sequence (GTTCAGTG), was also cloned into a luciferase reporter plasmid. AAV8-mIhh, AAV8-Alb-mTaz and control virus were from Vector Biolabs (AAV-278648, AAV-276356). AAV8 containing hepatocyte-specific TBG-Cre recombinase (AAV-TBG-Cre, AV-8-PV1091) and the control vector, AAV-TBG-LacZ (AV-8-PV0142), were purchased from the Penn Vector Core.

Histopathologic Analysis, Immunohistochemistry, and Immunofluorescence Microscopy

Formalin-fixed, paraffin-embedded human liver sections were stained with hematoxylin and eosin (H&E) and evaluated for severity of NAFLD by a trained hepatopathologist blinded to the clinical diagnosis, according to criteria described by Brunt et al. (Kleiner et al., 2005; Liang et al., 2014). TAZ^+ cells were quantified in immunostained human liver section images as the percentage of TAZ^+ cells per total DAPI-stained cells. Seven subjects in each NAFLD group were evaluated, and for each subject, 6-8 liver sections were analyzed. For mouse studies, inflammatory cells in H&E-stained liver section images were quantified as the number of mononuclear cells per field (10x objective). For most experiments, $F4/80^+$ cells were quantified in immunostained liver section images as the percentage of $F4/80^+$ cells per total DAPI-stained cells. For other parameters involving various stains, computerized image analysis (ImageJ) was used to quantify the area stained as stained area as a percentage of the total area of view; the same threshold settings were used for all analyses. For all analyses, we quantified 8 randomly chosen fields per section using 3 sections per mouse, with 1 mm between sections. NASH score (steatosis and inflammation) and fibrosis stage (modified Brunt) were assessed by a trained hepatopathologist blinded to the identity of the samples. Liver fibrosis was assessed by Picrosirius (Sirius) red (Polysciences, #24901) or by Masson's trichrome staining (Sigma, HT15), with aniline blue-positive areas quantified as a measure of collagen content in the trichrome-stained sections. TUNEL staining was conducted using a kit from Roche (#12156792910). For immunofluorescence microscopy, paraffin sections were rehydrated, subjected to antigen retrieval by placing in a pressure cooker for 10 mins in Target Retrieval Solution (Dako, S1699), and then blocked with serum. Sections were labeled with primary antibodies overnight, using a 1:150 dilution except for α-SMA and 4-HNE (1:200) and TAZ (1:100), followed by incubation with a fluorophore-conjugated secondary antibody for 1 h. The stained sections were mounted with DAPI-containing mounting medium (Life Technologies, P36935) and then viewed on an Olympus IX 70 fluorescence microscope. For filipin (Sigma, F9765) staining, frozen sections were fixed in 4% paraformaldehyde for 1 h at room temperature, then rinsed using glycine/PBS and stained 0.25 mg/ml filipin 2 h at room temperature. Fluorescence microscopic images were analyzed using ImageJ software. For immunohistochemistry, the deparaffinization, rehydration, and antigen retrieval processes were the same as with immunofluorescence staining. The slides

were treated with 3% hydrogen peroxide for 10 min and then blocked with Serum-Free Protein Block (Dako, X0909) for 30 min. Sections were incubated overnight with antibodies against TAZ, OPN, F4/80, or α-SMA (1:100) and then developed using DAB substrate kit (Cell Signaling, #8059) for TAZ, OPN and F4/80, HRP-labeled anti-FITC secondary antibody for α-SMA.

Measurement and Analysis of Liver Tissue Fatty Acids and Cholesterol

Liver specimens (~20 mg) were homogenized in 600 µl of 5% ethanol, and then 6 µl was added to 100 µl KOH (1M, 9:1 methanol:H_2O). The suspension was heated at 100^oC for 30 min and then clarified by centrifugation, followed by addition of 80 µl HCl to the supernate. Fatty acids in this solution were identified and quantified by gas chromatography in the Columbia Biomarker Core Laboratory. For liver cholesterol quantification, liver tissue was homogenized in H_2O. Color Reagent Solution from the Wako Total Cholesterol assay kit was added at a 1:20 ratio (v/v) to the liver lysates. The suspension was then centrifuged, and the supernates were read in a plate reader.

Immunoblotting

Liver protein was extracted using RIPA buffer (Thermo, #89900), and the protein concentration was measured by a BCA assay (Thermo, #23227). Proteins were separated by electrophoresis on 4-20% Tris gels (Life technologies, EC60285) and transferred to a nitrocellulose membranes (Bio-Rad, #1620115). The membranes were blocked for 30 min at room temperature in Tris-buffered saline and 0.1% Tween 20 (TBST) containing 5% (wt/vol) nonfat milk and then incubated with primary antibody in the same buffer at 4°C overnight, using 1:1000 dilution except for CHOP and Ihh (1:3000). The protein bands were detected with horse radish peroxidase-conjugated secondary antibodies (Cell Signaling) and Supersignal West Pico enhanced chemiluminescent solution (Thermo, #34080). Cultured cells were lysed in Laemmli sample buffer (Bio-Rad, #161-0737) containing 5% 2-mercaptoethanol, heated at 100ºC for 5 min, and then electrophoresed and immunoblotted as above. Preparation of nuclear and cytoplasmic fractions of liver was carried out using Nuclear Extract Kit (Active Motif, #40010) according to the manufacturer's protocol.

Cell Culture and Cell Isolation

AML12 mouse hepatocytes were purchased from ATCC (CRL-2254) and cultured in DMEM/F12 medium (Life Technologies, #11320) with 10% FBS (Gibco, #16140-071).

Hepatic stellate cells (HSCs) were isolated from 5-6 mo/o BALB/C mice as described previously (Mederacke et al., 2015). Briefly, after cannulation of the inferior vena cava, the portal vein was cut, allowing retrograde step-wise perfusion with solutions containing protease (Sigma Aldrich, P5147) and collagenase D (Roche, #11088866001). The perfusates were subjected to 9.7% Nycodenz (Accurate Chemical, #1002424) gradient centrifugation to isolate the HSCs, which were then plated in tissue culture dishes and used the next day. For conditioned medium transfer experiments, AML12 cells were cultured in DMEM containing 0.2% BSA and incubated for 24h. The media were then transferred to HSCs that had previously been incubated in DMEM, 0.2% BSA for 24 h. After 72 h, the HSCs were assayed for gene expression. For quantification of Ihh, hepatocyte conditioned medium was concentrated 10-fold by centrifugal filters (Millipore, Ultracel) and analyzed by an ELISA kit (LifeSpan Biosciences, F7953). Hepatocytes and combined non-hepatocyte cells were isolated from 10-week FPC-fed C57BL/6J mice. Hepatocytes were isolated as described previously (Ozcan et al., 2012). Combined non-hepatocyte cells used a similar protocol for liver cell suspension and then separated from hepatocytes using 14.5% Nycodenz gradient centrifugation. The purity of the preparations was assessed by immunoblot marker analysis.

Quantitative RT-qPCR

Total RNA was extracted from liver tissue or primary cultured hepatocytes using the RNeasy kit (Qiagen, 74106). cDNA was synthesized from 1 μg total RNA using oligo (dT) and Superscript II (Invitrogen). qPCR was performed with an 7500 Real time PCR system (Applied Biosystems) using SYBR green chemistry (Life Technologies, #4367659). The primer sequences are listed in **Table S4**.

siRNA-Mediated Gene Silencing and Transfection

siRNA sequences against mouse *Taz* and scrambled RNA were purchased from IDT. The target sequence of mouse *Taz* siRNA was ACA UGG ACG AGA UGG AUA CAG GUG A; the target sequence of mouse Ihh siRNA was UGC GGA CAA UCA UAC AGA ACC AGC A; and the target sequence of human *Taz* siRNA was GGA UAC UAG UUG UGA AAU GGA AAG A. siRNA and scrambled control RNA were transfected into AML12 cells (ATCC) using RNAiMAX (Life Technologies, #13778150) according to the manufacturer's instruction. A plasmid encoding GFP was purchased from Lonza (pmaxGFP), and a plasmid encoding murine *Ihh* was purchased from Origene

(MR227435). The plasmids were transfected into AML12 cells using Lipofectamine® LTX Reagent with PLUS™ Reagent (Life Technologies, #15338100).

Mouse Liver Nuclei Preparation and ChIP Assays

Mouse liver tissues were homogenized using a Dounce homogenizer (Wheaton, #357544) with a loose pestle in 1:10 (w:v) of ice-cold NP-40 lysis buffer supplemented with a protease inhibitor cocktail. The release of nuclei from the homogenate was monitored by DAPI staining and fluorescence microscopy. To purify intact nuclei, lysates were layered over a step gradient consisting of 1 M and 0.68 M sucrose and then centrifuged at 4000 rpm for 30 min at 4°C. Following a washing step, nuclear pellets were cross-linked with 1% fresh formaldehyde in PBS for 10 min at room temperature. Cross-linking was terminated by addition of 200 mM Tris-HCl (pH 9.4) and 1 mM DTT, and after 10 mins the suspension was centrifuged at 2500 rpm for 15 min at 4°C. Nuclear pellets were suspended in SDS lysis buffer containing protease inhibitors, incubated for 10 min on ice. DNA was sheared in a cold water bath using a focused-ultrasonicator (Covaris, S2) to obtain DNA fragments with an average size of 500 bps. Fragmented chromatin was pre-cleaned by incubating with normal rabbit IgG (Santa Cruz, sc-2027) for 1 h at 4 °C, followed by 1 h of incubation with 50 µL protein G magnetic beads (Pierce, #88847) at 4 °C with rotation. Immunoprecipitation was conducted using a rabbit anti-TAZ antibody (Cell Signaling, #4883), and a control rabbit anti-HA antibody (Santa Cruz, sc-805) was used as a negative control. Immunoprecipitated chromatin fragments were reverse cross-linked, digested by proteinase K, and purified using QIAquick PCR Purification Kit (Qiagen, #28106). The presence of TAZ in *Ihh* intronic region was quantified by qPCR and expressed relative to the input genomic DNA. The sequences of primers used for the ChIP-qPCR assays, including negative control primers, are descried in **Table S4**.

Luciferase Reporter Assays

Transient transfection of firefly and renilla luciferase reporter plasmids were carried out with Lipofectamine LTX & PLUS transfection reagent (ThermoFisher Scientific, #15338100). The level of promoter activity was evaluated by measuring firefly luciferase activity relative to renilla luciferase activity using the Dual Luciferase Assay System, as described by the manufacturer (Promega, E1910). A minimum of six independent transfections was performed and all assays were replicated twice.

Measurement of Hydroxyproline Content of Liver Tissue

Hydroxyproline liver content was measured as previously described (Bataller et al., 2003; Seki et al., 2009). Briefly, liver tissue was homogenized, and proteins were precipitated using trichloroacetic acid. Samples were hydrolyzed by incubation with 6N hydrochloric acid at 110°C for 16 h followed by neutralization with sodium hydroxide. Liver hydrolysates were oxidized using chloramine-T, followed by incubation with Ehrlich's perchloric acid reagent for color development. Absorbance was measured at 560 nm, and hydroxyproline quantities were calculated by reference to standards processed in parallel. Results are expressed as ng per mg liver weight.

HSC Proliferation Assay

Proliferation of HSCs was measured using the WST-1 cell proliferation kit (Sigma, #5015944001). HSCs in 96-well plates were cultured for 72 h in DMEM/10% FBS, and then siTaz or control scrambled RNA was added for 6 h. The cells were then cultured overnight in fresh DMEM/10% FBS, followed by culturing in DMEM/0.2% FBS for an additional 24 h. The media were then changed to DMEM/10% FBS, and after 48 h, the WST-1 reagent was added for 4 h, followed by assaying absorbance at 440 nm with a plate reader.

Supplemental References

Bataller, R., Schwabe, R.F., Choi, Y.H., Yang, L., Paik, Y.H., Lindquist, J., Qian, T., Schoonhoven, R., Hagedorn, C.H., Lemasters, J.J., et al. (2003). NADPH oxidase signal transduces angiotensin II in hepatic stellate cells and is critical in hepatic fibrosis. J Clin Invest *112*, 1383-1394.

Chang, T.C., Wentzel, E.A., Kent, O.A., Ramachandran, K., Mullendore, M., Lee, K.H., Feldmann, G., Yamakuchi, M., Ferlito, M., Lowenstein, C.J., et al. (2007). Transactivation of miR-34a by p53 broadly influences gene expression and promotes apoptosis. Mol Cell *26*, 745-752.

Kleiner, D.E., Brunt, E.M., Van Natta, M., Behling, C., Contos, M.J., Cummings, O.W., Ferrell, L.D., Liu, Y.C., Torbenson, M.S., Unalp-Arida, A., et al. (2005). Design and validation of a histological scoring system for nonalcoholic fatty liver disease. Hepatology *41*, 1313-1321.

Liang, W., Menke, A.L., Driessen, A., Koek, G.H., Lindeman, J.H., Stoop, R., Havekes, L.M., Kleemann, R., and van den Hoek, A.M. (2014). Establishment of a General NAFLD Scoring System for Rodent Models and Comparison to Human Liver Pathology. PloS one *9*, e115922.

Mederacke, I., Dapito, D.H., Affo, S., Uchinami, H., and Schwabe, R.F. (2015). High-yield and high-purity isolation of hepatic stellate cells from normal and fibrotic mouse livers. Nat Protoc *10*, 305-315.

Ozcan, L., Wong, C.C., Li, G., Xu, T., Pajvani, U., Park, S.K., Wronska, A., Chen, B.X., Marks, A.R., Fukamizu, A., et al. (2012). Calcium signaling through CaMKII regulates hepatic glucose production in fasting and obesity. Cell Metab *15*, 739-751.

Seki, E., De Minicis, S., Gwak, G.Y., Kluwe, J., Inokuchi, S., Bursill, C.A., Llovet, J.M., Brenner, D.A., and Schwabe, R.F. (2009). CCR1 and CCR5 promote hepatic fibrosis in mice. J Clin Invest *119*, 1858-1870.